

# Molecular line study of massive star forming regions from the RMS survey

Naiping Yu<sup>1,2,3\*</sup> and Jun-Jie Wang<sup>1,2\*†</sup>

<sup>1</sup>National Astronomical Observatories, Chinese Academy of Sciences, Beijing 100012, China

<sup>2</sup>NAOC-TU Joint Center for Astrophysics, Lhasa 850000, China

<sup>3</sup>Graduate School of the Chinese Academy of Sciences, Beijing 100080, China

Accepted 20\*\* December 15. Received 20\*\* December 14

## ABSTRACT

In this paper we selected a sample of massive star forming regions from the Red MSX Source (RMS) survey, to study star formation activities (mainly outflow and inflow signatures). We focused on three molecular lines from the Millimeter Astronomy Legacy Team Survey at 90 GHz (MALT90): HCO<sup>+</sup>(1-0), H<sup>13</sup>CO<sup>+</sup>(1-0) and SiO(2-1). According to previous observations, our sources could be divided into two groups: nine massive young stellar object (MYSO) candidates (radio-quiet) and ten HII regions (having spherical or unresolved radio emissions). Outflow activities were found in eleven sources while only three show inflow signatures in all. The high outflow detection rate means outflows are common in massive star forming regions. The inflow detection rate was relatively low. We suggest this was due to beam dilution of the telescope. All the three inflow candidates have outflow(s). The outward radiation and thermal pressure from the central massive star(s) do not seem to strong enough to halt accretion in G345.0034-00.2240. Our simple model of G318.9480-00.1969 shows it has an infall velocity of about 1.8 km s<sup>-1</sup>. The spectral energy distribution (SED) analysis agrees our sources are massive and intermediate-massive star formation regions.

**Key words:** ISM: molecules - ISM: outflows and inflow - ISM: structure - stars: formation - stars: protostars

## 1 INTRODUCTION

Massive stars have a deep impact on the evolution of galaxies. Despite of their short lives, they determine the main chemical and physical properties of the nearby interstellar medium (ISM). Both theories and observations demonstrate they could hamper or trigger the next generation of star formation, by the expansion of HII regions and supernova explosions at the end of their lives (e.g. Elmegreen & Lada 1977; Lefloch & Lazareff 1994). However, their formation mechanism is still poorly understood as they used to form in clusters, and detail study of massive star formation is further hampered by their short lives, far distances, rare sources and extensive dust extinctions. Several mechanisms have been proposed that high-mass stars could form by accretion through massive disks (e.g. Keto et al. 2002), competitive accretions in dense clusters (Bonnell et al. 2004), ionized accretion (Keto & Wood, 2006), and mergers of several low-mass stars (Bonnell et al. 1998). The former three models are similar to that of low-mass star formation, accompanied by outflow during the process of gravitational collapse. Recent observations appear to favor the former three mechanism as stellar mergers require a high stellar density of  $\geq 10^8$  stars

pc<sup>-3</sup>, which is more than 4 orders of magnitude larger than those found in young embedded dense clusters (Bonnell 2002). Given the accretion timescales in massive star-forming regions are much shorter than those in low mass star-forming regions, the inside nuclear burning of hydrogen takes place while massive stars are still accreting, which means there is no pre-main-sequence stage for massive stars. Then substantial UV photons and ionized stellar winds rapidly ionize the surrounding hydrogen, forming a hypercompact HII region (HCHII) or ultracompact HII region (UCHII). Many questions are still unclear: whether accretion could be halted by the strong outward radiation and thermal pressure. Does it continue in an ionized form? Does it continue through a molecular or ionized disk?

In recent years, using color selection criteria and the IRAS point source catalogue, several attempts have been taken to search for MYSOs (e.g. Molinari et al. 1996; Sridharan et al. 2002). However, because of the large IRAS beam ( $\sim 3\text{'}$  at 100  $\mu\text{m}$ ), these selected samples tend to be biased towards bright, isolated sources and avoid dense clustered environments at the Galactic mid-plane. By comparing the the colors of sources from the MSX and 2MASS point sources to those known MYSOs, Lumsden et al. (2002) identified approximately 2000 MYSO candidates. The Red MSX Source (RMS) survey is an ongoing multi-wavelength observational programme and will provide us the largest MYSO sample

\* E-mail: yunaiping09@mails.gucas.ac.cn

†

**Table 1.** List of our sources

MSX name	RA (J2000)	Dec. (J2000)	Type (candidate)	$V_{lsr}^a$ (km s <sup>-1</sup> )	$D^a$ (kpc)	H <sub>2</sub> O maser
G316.5871-00.8086	14:46:23.24	-60:35:47.0	MYSO	-45.8	3.2	Y
G318.9480-00.1969	15:00:55.31	-58:58:52.6	MYSO	-34.5	2.6	Y
G326.4755+00.6947	15:43:18.94	-54:07:35.4	MYSO	-41.6	1.8	Y
G326.5437+00.1684	15:45:53.26	-54:30:01.3	MYSO	-74.1	3.6	N
G326.6618+00.5207	15:45:02.84	-54:09:03.0	MYSO	-39.1	1.8	Y
G326.7796-00.2405	15:48:55.20	-54:40:37.7	MYSO	-64.7	3.6	Y
G329.0663-00.3081	16:01:09.93	-53:16:02.3	MYSO	-42.6	2.9	Y
G333.3151+00.1053	16:19:29.00	-50:04:40.9	MYSO	-47.4	4.0	Y
G345.5043+00.3480	17:04:22.87	-40:44:23.5	MYSO	-17.8	2.1	Y
G327.9018+00.1538	15:53:10.87	-53:39:58.1	HII	-93.1	5.8	N
G329.3371+00.1469	16:00:33.13	-52:44:47.1	HII	-107.1	7.3	Y
G332.8256-00.5498	16:20:10.46	-50:53:28.6	HII	-4.0	0.19	N
G336.9842-00.1835	16:36:12.42	-47:37:57.5	HII	-75.1	10.8	Y
G337.0047+00.3226	16:34:04.73	-47:16:29.2	HII	-62.8	10.8	N
G339.1052+00.1490	16:42:59.58	-45:49:43.6	HII	-78.2	4.9	N
G340.2480-00.3725	16:49:29.97	-45:17:44.4	HII	-50.3	3.9	N
G345.0034-00.2240	17:05:11.19	-41:29:06.3	HII	-28.7	2.9	N
G345.4881+00.3148	17:04:28.04	-40:46:23.3	HII	-17.6	2.1	N
G348.8922-00.1787	17:17:00.10	-38:19:26.4	HII	1.0	18.2	Y

a: Urquhart et al. (2007b; 2008)

for statistical studies. Using the Australia Telescope Compact Array (ATCA), Urquhart et al. (2007a) completed the 5 GHz observations of 892 RMS sources in the southern sky. This programme divided these sources into three groups: real MYSO candidates, HII regions (UCHII and HCHII) and others such as evolved stars and planetary nebulae (PNe). To obtain kinematic distances, Urquhart et al. (2007b; 2008) made <sup>13</sup>CO (1-0) and (2-1) observations at Mopra, Onsala and Purple Mountain Observatory (PMO) 13.7 m telescope, and the 15 m James Clerk Maxwell Telescope (JCMT), as well as archival data extracted from the Galactic Ring Survey (GRS). They found that the majority of these sources have multiple velocity components along each line of sight. The multiple emission features make it difficult to assign a unique kinematic velocity to each source. In order to identify a more reliable molecular component, they further searched archival water and methanol masers catalogues of Valdetaro et al. (2001) and Pestalozzi et al. (2005), less abundant but denser gas molecular traces like CS (2-1) observations by Bronfman et al. (1996). And then by using the rotation curve of Brand and Blitz (1993) and their radial velocities, kinematic distances for all detected components can be derived. Based on the above observations and research, we selected about twenty RMS sources to study star formation activities (mainly outflow and inflow signatures) using data from Millimeter Astronomy Legacy Team 90 GHz survey (MALT90). We present the introductions of our data and source selections in section 2, results and analysis in section 3, and summary in section 4.

## 2 DATA AND SOURCE SELECTIONS

The MALT90 is a large international project aimed at characterizing the sites within our Galaxy where high-mass stars will form. Exploiting the unique broad frequency range and fast-mapping capabilities of the Mopra 22-m telescope, MALT90 maps 16 emission lines simultaneously at frequencies near 90 GHz. These molecular lines will probe the physical, chemical, and evolutionary states of

dense high-mass star-forming cores. We focused on three molecular lines from the MALT90 Survey: HCO<sup>+</sup>(1-0), H<sup>13</sup>CO<sup>+</sup>(1-0) and SiO(2-1). HCO<sup>+</sup> often shows infall signatures and outflow wings (e.g., Rawlings et al. 2004; Fuller et al. 2005). H<sup>13</sup>CO<sup>+</sup>(1-0) provides optical depth and line profile information. SiO (2-1) is seen when SiO is formed from shocked dust grains, typically in outflows (Schilke et al. 1997). The survey covers a Galactic longitude range of  $\sim -60$  to  $\sim 15^\circ$  and Galactic latitude range of  $-1$  to  $+1^\circ$ . The observations were carried out with the newly upgraded Mopra Spectrometer (MOPS). The full 8 GHz bandwidth of MOPS was split into 16 zoom bands of 138 MHz each providing a velocity resolution of  $\sim 0.11$  km s<sup>-1</sup>. The angular resolution of Mopra is about 38 arcsec, with beam efficiency between 0.49 at 86 GHz and 0.42 at 115 GHz (Ladd et al. 2005). The maps were made with 9'' spacing between adjacent rows. More information about this survey can be found in Foster et al. (2011) and Hoq et al. (2013). The MALT90 data includes ( $l, b, v$ ) data cubes and ( $l, b$ ) moment and error maps, and is publicly available from the MALT90 Home Page<sup>1</sup>. The data processing was conducted using CLASS (Continuum and Line Analysis Single-Disk Software) and GreG (Grenoble Graphic) software packages.

In order to study massive star formation activities (mainly outflow and inflow signatures), we selected nineteen sources from the RMS survey by applying the following criteria: (1) Sources should not be on the edge of known HII or supernova regions, considering the large beam of the 22 m Mopra telescope; (2) According to the observations of ATCA (Urquhart et al. 2007a), sources should be radio quiet or have a simple spherical/unresolved radio emissions; (3) All sources should be detected by MALT90; (4) The LSR velocities of HCO<sup>+</sup> and H<sup>13</sup>CO<sup>+</sup> should be the same as Urquhart et al. (2007b; 2008). We need to mention here that our sample is not complete according to the above four criteria. We wish a much more complete research of the RMS sources by the MALT90 data in the

<sup>1</sup> See <http://atoa.atnf.csiro.au/MALT90>

**Table 2.** Outflow parameters

Source	Shift	$\Delta v$ (Km s <sup>-1</sup> )	N (HCO <sup>+</sup> ) ( $\times 10^{12}$ cm <sup>-2</sup> )	M (M <sub>⊙</sub> )	$P_{out}$ (M <sub>⊙</sub> km s <sup>-1</sup> )	$E_{out}$ (M <sub>⊙</sub> [km s <sup>-1</sup> ] <sup>2</sup> )
G326.4755+00.6947	red	(-40, -33)	22.4	16.8	118	412
	blue	(-47, -42)	17.7	19.0	95	238
G326.7796-00.2405	red	(-64, -62)	10.0	21.4	43	43
	blue	(-69, -66)	8.91	23.9	72	108
G333.3151+00.1053	red	(-45.3, -44)	4.8	15.2	20	13
	blue	(-50, -47)	11.8	46.8	140	211
G345.5043+00.3480	red	(-12, -15)	12.2	6.7	20	30
	blue	(-20, -24)	9.1	10.0	40	80
G329.3371+00.1469	red	(-106, -104)	8.9	78.4	157	157
	blue	(-112, -110)	5.6	49.3	99	99
G332.8256-00.5498	red	(-49 -53)	14.0	1.0	4	8
	blue	(-65, -61)	11.3	1.7	7	14
G340.2480-00.3725	red	(-49, -46)	9.5	50.2	151	226
	blue	(-56, -53)	10.7	65.9	198	297
G345.0034-00.2240 <sup>a</sup>	red	(-22, -19)	6.1	14.8	89	266
	blue	(-35, -31)	9.8	28.6	172	515
G345.4881+00.3148	red	(-15, -12)	14.0	21.6	65	97
	blue	(-22, -19)	21.8	28.6	86	129

a: The outflow parameters of this source are calculated by HNC(1-0).

near future. The information of our selected sources are listed in table 1. Nearly all of the MYSO candidates are associated with water masers according to former observations, however in the HII regions only three sources are associated with water maser emissions. This suggests in massive star formation regions, water masers are more likely to be associated with MYSOs than HII regions.

### 3 RESULTS AND DISCUSSIONS

Infall and outflow are two of the most important elements to understand the theories of massive star formation. Infall can act to replenish disk material as mass falls onto a protostar, while outflows serve as a release mechanism for the angular momentum that builds up during the accretion process. These motions can be studied by investigating the profiles of optically thick and optically thin molecular lines. Blue profile, a combination of a double peak with a brighter blue peak or a skewed single blue peak in optically thick lines, can be used to study infall motions (Sun et al. 2008). Surely blue profile may also be caused by rotation and outflow. However, infall motion is the only process that would produce consistently the blue profile. Outflow and rotation only produce a blue asymmetric line profile along a particular line of sight to a source (Sun et al. 2008).

SiO is also a well-known tracer of recent outflow. In the cold diffuse ISM, the element of Si is regarded to be frozen into dust grains. When the gas is shocked (i.e., the gas through which a protostellar outflow is passing) the dust grains can sublimate and Si is released into gas phase. Thus, the detections of SiO emissions from MYSOs could always be equal to the detections of recent outflow activities. In the following sections, we use position-velocity (PV) diagram of HCO<sup>+</sup> (1-0) and/or SiO (2-1) (if detected) to study outflows in our sample. For G318.9480-00.1969, we also employed

the three dimensional radiative-transfer code RADMC3D, developed by C. Dullemond<sup>2</sup>, to compute the HCO<sup>+</sup> (1-0) line emission from an infalling model.

#### 3.1 Outflow signatures detected by HCO<sup>+</sup> (1-0) and SiO (2-1)

Outflow makes an important contribution to the line wing emissions of HCO<sup>+</sup> (1-0), as it becomes optically thick quickly and readily self-absorbs in dense gas regions. We drew PV diagrams for our sources. According to the PV diagrams, we selected the integrated range of wings and determined the outflow intensities of red and blue lobes. Four HCO<sup>+</sup> (1-0) PV diagrams of our nine MYSO candidates and four in ten HII regions show distinct wing emissions (figure 1 and figure 2, respectively), which may be probably caused by bipolar outflows. Figure 3 and figure 4 show the integrated maps by integrating wing emissions of our MYSOs and HII regions, respectively. The Mopra beam size is 38'' and the spacing of the spectra is 9'', so there are about  $4 \times 4 = 16$  spectra within a single beam. In the sample of MYSOs, the peak emissions of red and blue lobes are within one beam and we could not determine the outflow directions. It also seems impossible that all the axis of these outflows are nearly parallel with the line of sight. By comparing figure 3 and figure 4, it can be noted that the MYSO outflows are more compact than those found in HII regions. Considering the mean distance of our RMS sources with radio emission ( $\sim 5.7$  kpc) is larger than those radio quiet ( $\sim 2.6$  kpc), our result agrees MYSO candidates should be in much earlier stage than HCHII/UCHII regions.

Figure 5 shows the five detected SiO spectra toward our sources. Among these five sources, three (G318.9480-00.1969, G326.4755+00.6947, G329.0663-00.3081) are MYSO candidates

<sup>2</sup> See <http://www.ita.uni-heidelberg.de/dullemond/software/radmc-3d/>

**Table 3.** SED parameters

RMS sources	Stellar mass [M <sub>⊙</sub> ]	Disk mass [M <sub>⊙</sub> ]	Envelope mass [M <sub>⊙</sub> ]	Total luminosity [L <sub>⊙</sub> ]	Best-fit model
G318.9480-00.1969	9.56	$4.68 \times 10^{-3}$	$9.65 \times 10^0$	$5.72 \times 10^3$	3014991
G326.4755+00.6947	10.10	$9.77 \times 10^{-3}$	$1.14 \times 10^3$	$9.06 \times 10^3$	3000136
G326.7796-00.2405	8.08	$4.58 \times 10^{-2}$	$2.68 \times 10^1$	$7.33 \times 10^2$	3004818
G329.0663-00.3081	9.49	$5.52 \times 10^{-2}$	$3.08 \times 10^1$	$1.45 \times 10^3$	3010080
G333.3151+00.1053	13.91	$5.88 \times 10^{-4}$	$6.46 \times 10^2$	$1.70 \times 10^4$	3000244
G345.0034-00.2240	9.67	$7.58 \times 10^{-2}$	$4.42 \times 10^1$	$7.81 \times 10^3$	3003254

and the other two (G340.2480-00.3725 and G345.0034-00.2240) are HII regions. Models and observations also suggest SiO emissions could be caused by photodissociated region (PDR) and not an outflow (e.g. Schilke et al. 2001; Shepherd et al. 2004). For the MYSO candidates, as they are radio quiet, SiO emissions triggered by PDR around HII regions are impossible. However, a PDR could also exist without the presence of ionized gas. Through the method described by Klaassen et al. (2007), we estimated the SiO column densities  $> 10^{14}$  cm<sup>-2</sup> of the five sources, much larger than those found in PDRs ( $\sim 10^{12}$  cm<sup>-2</sup>) (Schilke et al. 2001). We thus regard these SiO emissions are due to recent outflow activities.

We should mention that the outflow detection rate is just a low limit. One reason is due to the beam dilution, especially for the MYSO candidates. For example outflow activity was not found in MYSO G318.9480-00.1969 through PV diagram analysis, however the SiO emission discussed above shows recent outflow(s) in this region. Outflow(s) in this source may be very young and is thus heavily diluted. The other reason is due to the molecular line we used to trace outflow. Considering the wide range of physical conditions in star formation regions (i.e. gas densities from  $\sim 10^{-20}$  g cm<sup>-3</sup> to  $\sim 10^{-16}$  g cm<sup>-3</sup>, and gas temperatures from  $\sim 10$  K to  $\sim 100$  K), there is non-trivial molecular tracer to detect outflows in all conditions. For example, the PV diagram of HCO<sup>+</sup> in G345.0034-00.2240 does not show red-shifted emission wings (figure 6). The gas near -17 km/s is possibly unrelated to this source. However, when we chose HNC instead of HCO<sup>+</sup>, wing emissions caused by bipolar outflow was evident. Besides, the SiO spectra of G345.0034-00.2240 extends from -8 km s<sup>-1</sup> to -48 km s<sup>-1</sup>. The wide line emissions further suggest young outflow activities. PV diagram of SiO in G345.0034-00.2240 cut along east-west direction is shown in figure 7. Figure 7 also shows the maps of the integrated blue and red shifted SiO (2-1) emission (the dash contours). It can be noted SiO traces the inner region of the outflow, compared to HNC. The outflow detection rate by SiO in MYSOs ( $\sim 33$  %) is much higher than that in HII regions ( $\sim 20$  %). That is because SiO is particularly well suited to tracing recent outflows, as it persists in the gas phase for only  $\sim 10^4$  years after being released by shocks (e.g., Pineau des Forets et al. 1997).

Assuming that HCO<sup>+</sup> (1-0) emission in the line wings to be optically thin and Local Thermodynamic Equilibrium (LTE),  $X(\text{HCO}^+) = [\text{HCO}^+]/[\text{H}_2] = 10^{-8}$  (Turner et al. 1997) and  $T_{ex} = 15$  K, we derive the column density using:

$$N(\text{HCO}^+) = Q(T_{ex}) \frac{8\pi\nu_0^3}{c^3} \frac{g_l}{g_u A_{ul}} \frac{1}{[1 - e^{-h\nu_0/kT_{ex}}]^{-1}} \int \tau dv \quad (1)$$

where  $\nu_0$ ,  $g_u$ ,  $g_l$  and  $A_{ul}$  are the rest frequency, the upper and lower level degeneracies and the Einstein's coefficient of HCO<sup>+</sup>,  $Q(T_{ex})$  is the partition function, and  $c$  is the speed of light. In addition,

by assuming that the HCO<sup>+</sup> emission is optically thin in the line wings, we use the approximation:

$$\int \tau dv = \frac{1}{J(T_{ex}) - J(T_{bg})} \int T_{mb} dv \quad (2)$$

where  $T_{bg}$  is the temperature of the background radiation (2.73 K). Using  $M_{out} = \mu m_H d^2 \Omega X(\text{HCO}^+)^{-1} N(\text{HCO}^+)$ , we obtain the masses for the red and blue molecular outflows, where  $N(\text{HCO}^+)$  is the HCO<sup>+</sup> column density calculated through the above equations,  $d$  is the distance,  $\Omega$  is the area of the lobes (within 50% of each peak emission), and  $m_H$  is the hydrogen atom mass. We adopt a mean molecular weight per H<sub>2</sub> molecule of  $\mu = 2.72$  to include helium. We estimate the momentum and energy of the red and blue lobes using

$$P_{out} = M_{out} V \quad (3)$$

and

$$E_{out} = \frac{1}{2} M_{out} V^2 \quad (4)$$

where  $V$  is a characteristic velocity estimated as the difference between the maximum velocity of HCO<sup>+</sup> emission in the red and blue wings respectively, and the molecular ambient velocity ( $V_{lsr}$ ). The derived parameters are shown in table 2.

## 3.2 Infall

### 3.2.1 The blue profile

Previous studies show HCO<sup>+</sup> (1-0) is a good inward motion tracer in star formation regions (e.g. Sun et al. 2008). The five HCO<sup>+</sup> (1-0) emission lines of our sources (figure 8, right panels) are far of having a simple Gaussian shape, presenting asymmetries, and spectral wings or shoulders, which suggest that the molecular gas is affected by the dynamics of these star-forming regions. However, we know double peak could also be caused by two velocity components in the line of sight. The detections of optically thin molecular lines such as H<sup>13</sup>CO<sup>+</sup> (1-0) could help us to rule out this possibility. Mapping observations could help us to identify whether this was caused by inward motions or other dynamics such as outflow, rotation and expansions of HII regions. Figure 8 (the left panels) shows the mapping observations towards our sources with double peaked HCO<sup>+</sup> (1-0) emissions. All the spectra of H<sup>13</sup>CO<sup>+</sup> in figure 8 peaks near the dip of HCO<sup>+</sup>. Besides, three of them (G318.9480-00.1969, G345.0034-00.2240 and G345.4881+00.3148) show consistent blue profiles, indicating infall motions. To quantify the blue profile, we further used the asymmetry parameter  $\delta V$  defined as the difference between the peak velocities of an optically thick line  $V(\text{thick})$  and an optically thin line  $V(\text{thin})$  in units of the optically thin line FWHM (Full Width at Half Maximum)  $dV(\text{thin})$ :  $\delta V =$

$\frac{V(\text{thick})-V(\text{thin})}{dV(\text{thin})}$ . Mardones et al. (1997) adopted a criterion  $\delta V < -0.25$  to indicate blue asymmetry. Our calculations further demonstrate blue profiles caused by inflow in G318.9480-00.1969 ( $\delta V = -0.27$ ), G345.0034-00.2240 ( $\delta V = -0.63$ ) and G345.4881+00.3148 ( $\delta V = -0.37$ ). Outflow activities are also detected in these regions (see section 3.1). This suggests that like low star formation theories, massive stars in these regions are probably forming through accretion-outflow process. For G345.0034-00.2240, if the detection of recent outflow activity traced by SiO and the appearance to be undergoing infall are indeed caused by the central massive young star(s), this suggests the outward radiation and thermal pressure from the central massive star(s) do not strong enough to halt accretion. Like the case of G10.6-0.4 (Keto & Wood 2006), accretion flow in this region may be ionized. Given the low angular resolution of the data (at 2.9 kpc,  $38''$  is over half a parsec), it is also possible that a lower mass star is forming in the vicinity. Deeper observations should be carried out to study our speculation.

Sun et al. (2008) made single-pointing and mapping observations of  $\text{HCO}^+$  (1-0) from the 13.7m telescope of PMO. Among their 29 massive star-forming cores (mainly UCHII regions), six sources were identified to be strong infall candidates. The detection rate is consistent with our study, even though the resolution of Mopra is much higher than that of the 13.7m telescope ( $38''$  vs.  $58''$ ). This may be because all of their source distances are less than 4 kpc while half of our sources locate more than 5 kpc away. Klaassen et al. (2007,2012) also obtained JCMT observations of  $\text{HCO}^+/\text{H}^{13}\text{CO}^+$  (4-3) to trace large scale inward motions in a sample of massive star-forming regions (mainly MYSOs, HCHII and UCHII regions). The infall rate in our sample is relatively low compared with their work. This partly may be due to their higher resolution ( $15''$  vs.  $38''$ ). Besides, the  $J = 4-3$  transition is likely a better asymmetry tracer than  $J = 1-0$  (see figure 8 of Tsamis et al. 2008). Only one source in our MYSO candidates shows infall signature. This may be because the infall area within MYSO is relatively smaller than that in UCHII regions, and then more likely to be beam diluted.

### 3.2.2 A simple infall model of G318.9480-00.1969

G318.9480-00.1969 is the only MYSO candidate showing infall signature. In this section, in order to constrain the spatial and dynamic structures of G318.9480-00.1969, we constructed a radiative-transfer model that reproduces the observations. The three-dimensional radiative-transfer code RADMC-3D, developed by C. Dullemond, was employed to compute the dust temperature from stellar heating and the continuum and line emission of an infall model. The dust opacity is from Ossenkopf & Henning (1994) without grain mantles or coagulation. The molecular data of  $\text{HCO}^+$  comes from the Leiden LAMDA database<sup>3</sup>. The line transfer assumes the gas temperature to be equal to the dust temperature and LTE (full non-LTE radiation transfer is also planned for RADMC-3D).

In our model, the volume density follows a radial power law,  $n \propto r^{-1.5}$ , with a total mass of  $31 M_{\odot}$  (estimated from our observations) within a box of  $(4000 \text{ AU})^3$ . Inside there is a star of  $10 M_{\odot}$  (see section 3.3). The gas has a turbulence velocity of  $0.5 \text{ km s}^{-1}$  and is radially infalling with  $1.8 \text{ km s}^{-1}$  to the central star. The model is inevitably simplified. A comparison of the observed and

model spectra is shown in figure 9. At the center, the model spectra matches well with the observation. However, the observed line seems to have line wing emissions, probably caused by outflow activities. The detected SiO spectra in this region indeed implies beam diluted outflow(s). Even though our model is consistent with the data, we should realize it does not provide errors of the parameters, and different models may also fit as well. However, it provides us a way to study the structure of star forming regions.

### 3.3 Spectral energy distribution

In this section, we try to fit the spectral energy distribution (SED) of our sources using the tool developed by Robitaille et al. (2007). Briefly, the SED-fitting tool works as a regression method to find the SEDs within a specified  $\chi^2$  from a large grid of models after fitting the input data points. The grid of models contains stellar masses, disk masses, mass accretion rates, and line-of-sight (LOS) inclinations. The grid of YSO models was computed by Robitaille et al. (2006) using the 20,000 two-dimensional radiation transfer models from Whitney et al. (2003a, 2003b, 2004). Each YSO model has SEDs for 10 viewing angles (inclinations), so the total YSO grid consists of 200,000 SEDs. We use archival data from 2MASS, IRAC of Spitzer, MSX to fit the SED of our sources. In addition to the best-fit model (the black line in figure 10), we also show the range of possible parameters that can be derived from models within the range of  $\chi^2/\nu - \chi^2_{\text{best}}/\nu \leq 4$  ( $\nu$  represents the number of data points). The best derived model parameters are listed in table 3 and the resulting SEDs are shown in figure 10. Of these six sources, five are HII regions. This may be because the protostar(s) of MYSOs are still deeply imbedded, even infrared emissions are hard to be detected. The SED agrees our sources are massive and intermediate-massive star formation regions, with masses ranging from 8 to  $14 M_{\odot}$ .

## 4 SUMMARY

By analyzing  $\text{HCO}^+$ (1-0),  $\text{H}^{13}\text{CO}^+$ (1-0) and  $\text{SiO}$ (2-1) molecular data from MALT90, we studied the outflow and infall activities in nineteen RMS sources. The high outflow detection rate ( $\geq 58\%$ ) suggests that outflows are common in massive star forming regions as in low mass star forming regions. All of the detected outflows in our radio-quiet RMS sources are much more compact than those found in radio-loud RMS sources, indicating they are at earlier stages. The outward radiation and thermal pressure from the central massive star(s) of G345.0034-00.2240 do not seem to strong enough to halt accretion in this region. The detection of recent outflow activity traced by SiO and the appearance to be undergoing infall in this region suggest ionized accretion flow can continue through an HII region and massive star(s) in this region could be formed through ionized accretions. Only one source of our MYSO candidates shows infall signature. This may be because the infall area with MYSO is relatively small, and thus more likely to be beam diluted. A simple model of G318.9480-00.1969 shows it has an infall velocity of about  $1.8 \text{ km s}^{-1}$ . The spectral energy distribution (SED) further agrees our RMS sources are massive and intermediate-massive star formation regions.

<sup>3</sup> <http://www.strw.leidenuniv.nl/~moldata>

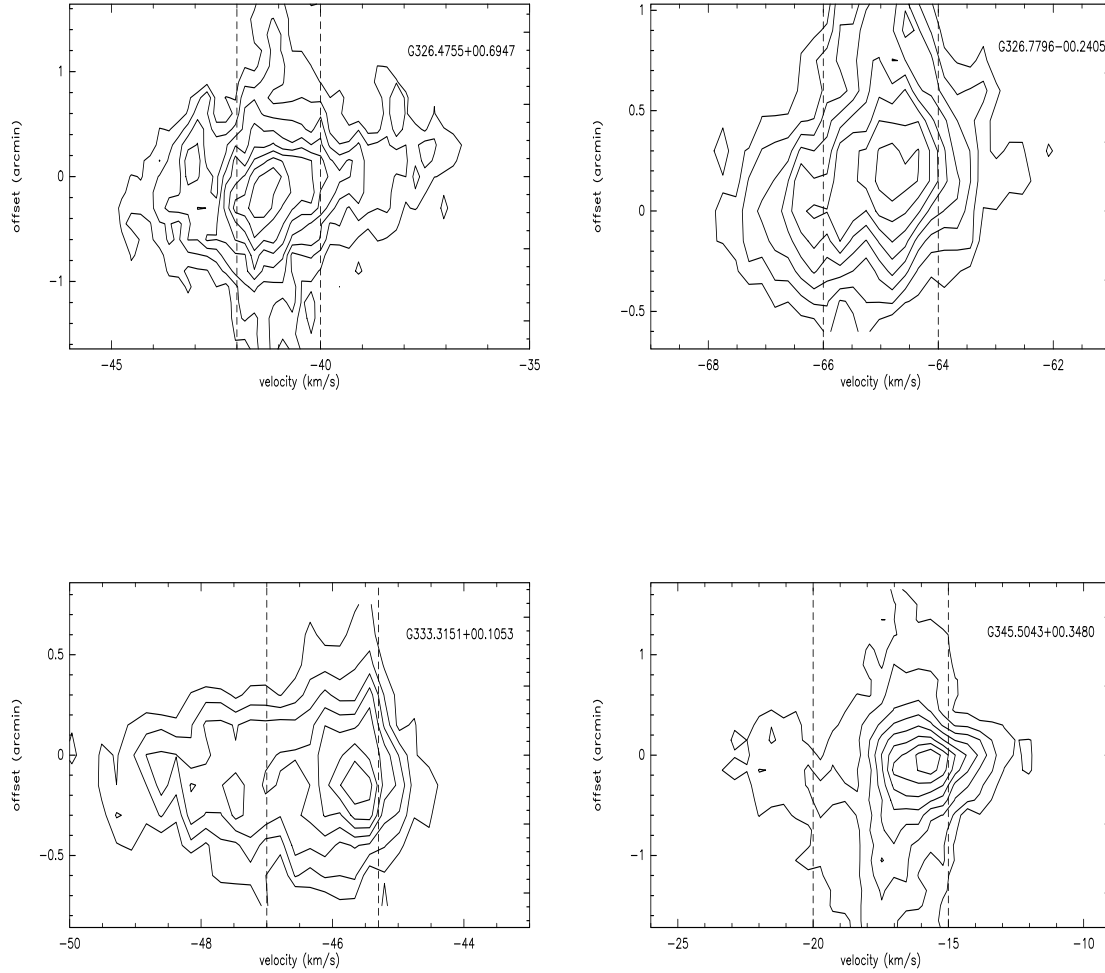


**Figure 1.** PV diagrams of the MYSO candidates show HCO<sup>+</sup> (1-0) wing emissions. Contours are 20%, 30%...90% of the peak emissions. The dashed lines indicate the velocity ranges for the blue and red wings as listed in table 2.

## 5 ACKNOWLEDGEMENTS

We thank the anonymous referee for constructive suggestions. This paper made use of information from the Red MSX Source (RMS) survey database [http://rms.leeds.ac.uk/cgi-bin/public/RMS\\_DATABASE.cgi](http://rms.leeds.ac.uk/cgi-bin/public/RMS_DATABASE.cgi) which was constructed with support from the Science and Technology Facilities Council of the UK. This research made use of data products from the Millimetre Astronomy Legacy Team 90 GHz (MALT90) survey. The Mopra telescope is part of the Australia Telescope and is funded by the Commonwealth of Australia for operation as National Facility managed by CSIRO.

## REFERENCES

- Bonnell, I.A. et al 1998, MNRAS, 298, 93  
 Bonnell, I.A. 2002, in ASP Conf.Ser. 267, The Earliest Stages of Massive Star Birth, ed. P.A. Crowther (San Francisco: ASP), 193

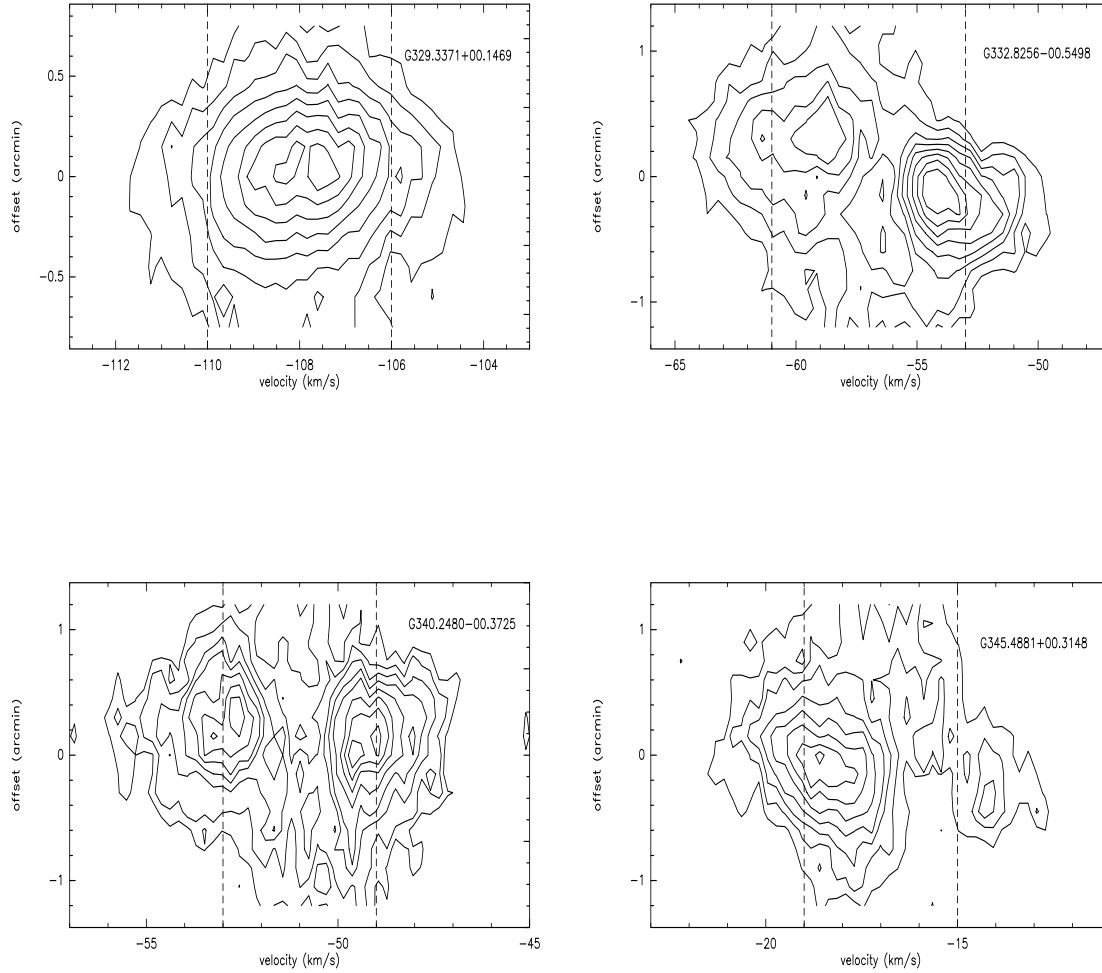


**Figure 2.** PV diagrams of the HII candidates show HCO<sup>+</sup> (1-0) wing emissions. Contours are 20%, 30%...90% of the peak emissions. The dashed lines indicate the velocity ranges for the blue and red wings as listed in table 2.

Bonnell, I.A. et al. 2004, MNRAS, 349, 735  
 Bronfman, L., Nyman, L.-A., May, J., 1996, A&AS, 115, 81  
 Elmegreen, B. G., Lada C.J., 1977, ApJ, 214, 725  
 Foster J.B., et al. 2011, ApJS, 197, 25  
 Fuller, G. A., Williams, S. J., Sridharan, T. K., 2005, A&A, 442, 949  
 Hoq, S., Jackson, J.M., Foster, J.B., et al. 2013, ApJ, 777, 157  
 Keto, E. 2002, ApJ, 580, 980  
 Keto, E., Wood, K. 2006, ApJ, 637, 850  
 Klaassen, P.D., Wilson, C.D., 2007, ApJ, 663, 1092  
 Klaassen, P.D., Testi, L., Beuther, H., 2012, A&A, 538, 140  
 Ladd, N., Purcell, C., Wong, T., & Robertson, S. 2005, PASA, 22, 62  
 Lefloch, B., Lazareff, B., 1994, A&A, 289, 559  
 Lumsden, S. L., Hoare, M. G., Oudmaijer, R. D., Richards, D. 2002, MNRAS, 336, 621  
 Mardones, D., Myers, P. C., Tafalla, M. et al. 1997, ApJ, 489, 719  
 Molinari, S., Brand, J., Cesaroni, R., Palla, F. 1996, A&A, 308, 573  
 Ossenkopf, V., & Henning, T. 1994, A&A, 291, 943  
 Pestalozzi, M.R., Minier, V., Booth, R.S., 2005, A&A, 432, 737

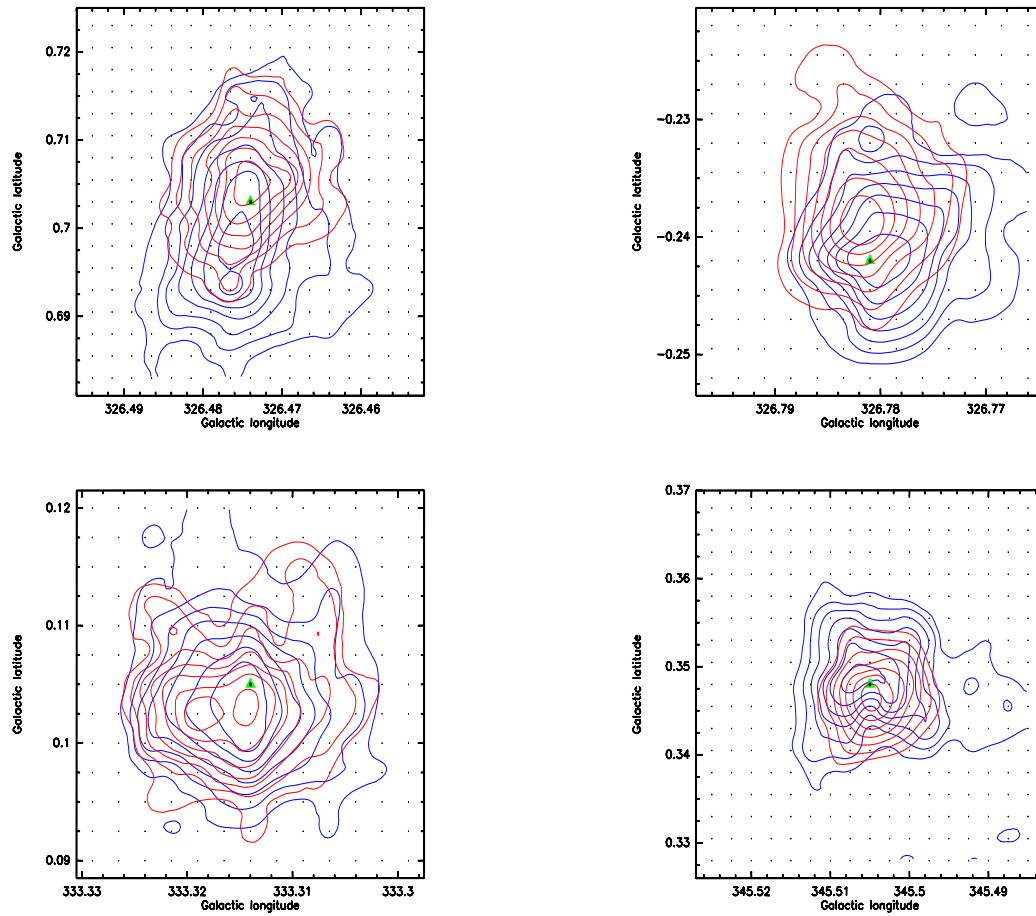


**Figure 3.** The blue and red contours show the  $\text{HCO}^+$  (1-0) integrated wing emissions of the MYSO candidates. The green triangles mark the RMS sources and the dot symbols mark the mapped points. The levels are 30%, 40%...90% of the peak emissions respectively.

- Pineau des Forets, G., Flower, D. R., & Chieze, J.-P. 1997, in IAU Symp. 182, Herbig-Haro Flows and the Birth of Stars, ed. B. Reipurth & C. Bertout (Dordrecht: Kluwer), 199
- Rawlings, J. M. C., Redman, M. P., Keto, E., Williams, D. A., 2004, MNRAS, 351, 1054
- Robitaille, T. P., Whitney, B. A., Indebetouw, R., Wood, K., Denzmore, P., 2006, ApJS, 167, 256
- Robitaille, T. P., Whitney, B. A., Indebetouw, R., Wood, K., 2007, ApJS, 169, 328
- Schilke, P., Walmsley, C. M., Pineau des Forets, G., Flower, D. R., 1997, A&A, 321, 293
- Schilke, P., Pineau des Forêts, G., Walmsley, C.M., et al., 2001, A&A, 372, 291
- Shepherd, D.S., Kurtz, S.E., Testi, L. 2004, ApJ, 601, 952
- Sridharan, T. K., Schilke, P., Menten, K. M., Wyrowski, F. 2002, ApJ, 566, 931
- Sun Yan, Gao Yu, 2008, MNRAS, 392, 170
- Tsamis, Y.G., Rawlings, J.M.C., Yates, J.A., Viti, S. 2008, MNRAS, 388, 898
- Urquhart, J. S., Busfield, A. L., Hoare, M. G., et al. 2007a, A&A, 461, 11
- Urquhart, J. S., et al. 2007b, A&A, 474, 891
- Urquhart, J. S., et al. 2008, A&A, 487, 253
- Valdettaro, R., Palla, F., Brand, J., et al. 2001, A&A, 368, 845
- Whitney, B. A., Indebetouw, R., Bjorkman, J.E., Wood, K., 2004, ApJ, 617, 1177
- Whitney, B. A., Wood, K., Bjorkman, J. E., Cohen, M., 2003a, ApJ, 598, 1079
- Whitney, B. A., Wood, K., Bjorkman, J. E., Wolff, M. J., 2003b, ApJ, 591, 1049



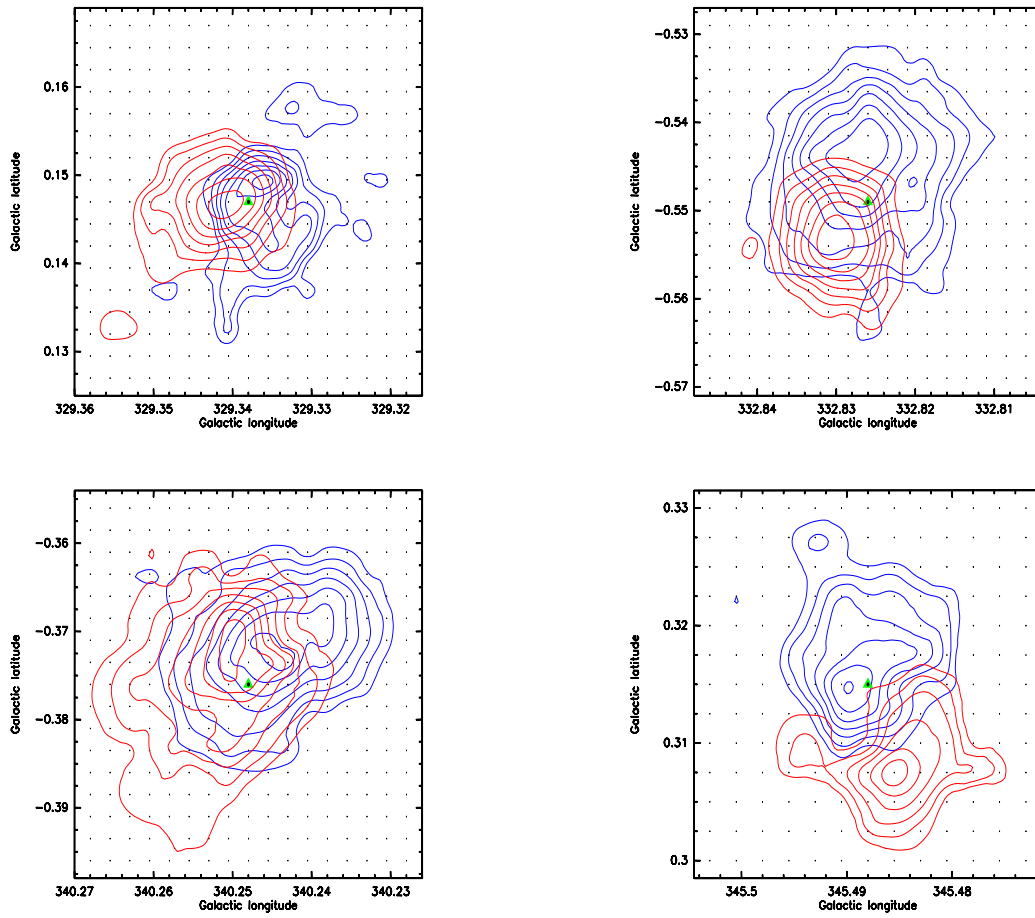


**Figure 4.** The blue and red contours show the HCO<sup>+</sup> (1-0) integrated wing emissions of the HII candidates. The green triangles mark the RMS sources and the dot symbols mark the mapped points. The levels are 30%, 40%...90% of the peak emissions respectively.

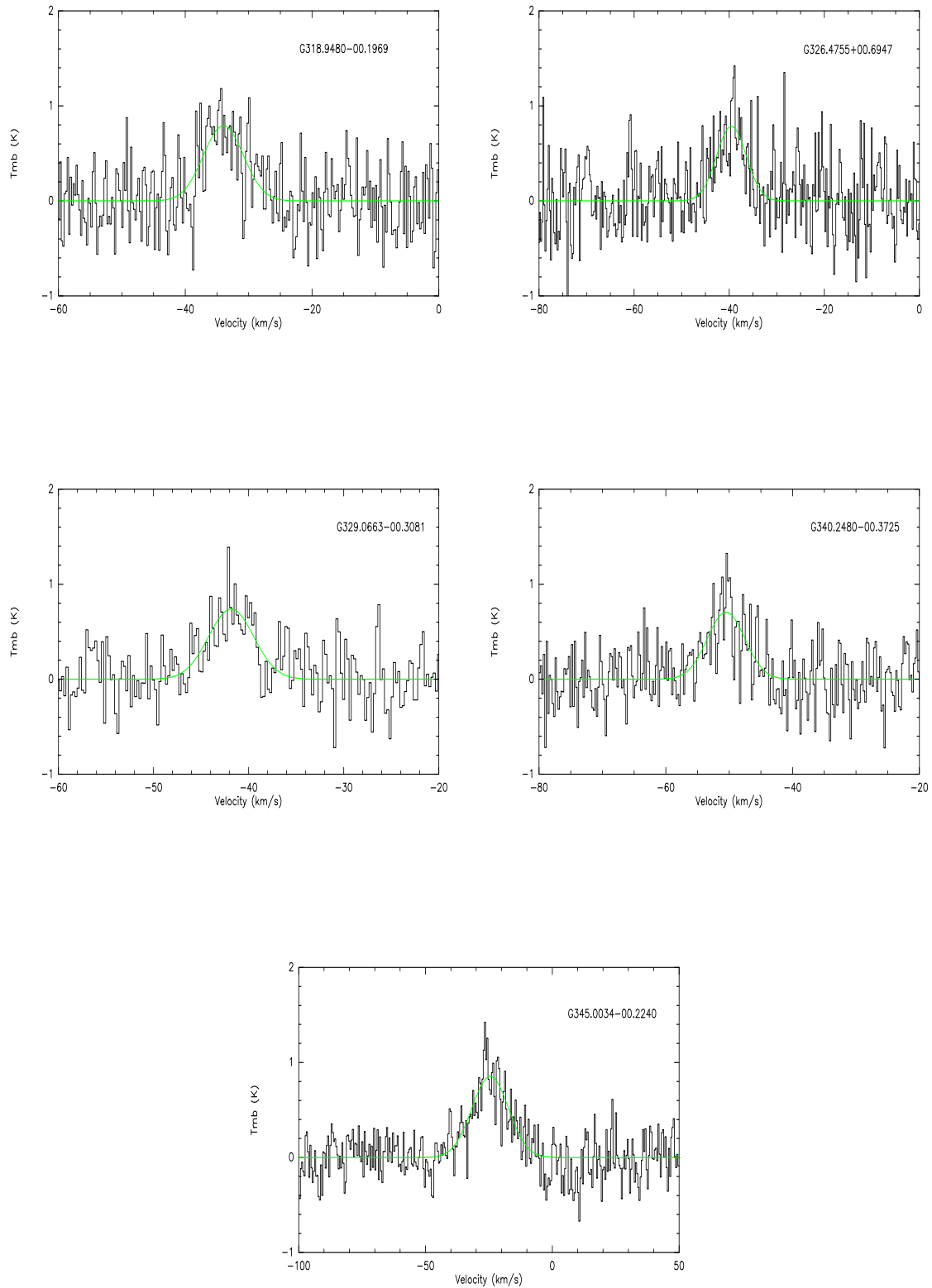


**Figure 5.** SiO (2-1) spectra for five sources in which SiO was detected. The green lines are the Gaussian-fitted lines.

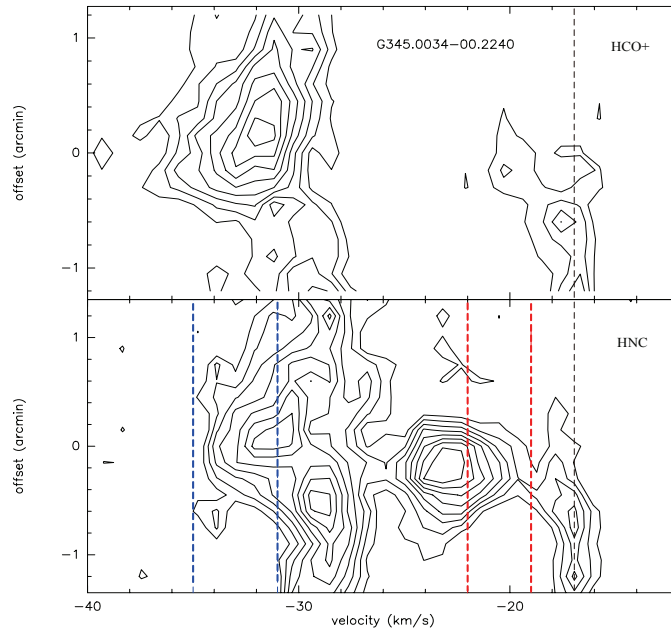


**Figure 6.** PV diagrams made by HCO<sup>+</sup> (top) and HNC (bottom) of G345.0034-00.2240. Contours are 20%, 30%...90% of the peak emissions. The red and blue dashed lines indicate the velocity ranges for the blue and red wings as listed in table 2. The gas at -17 km/s is possibly unrelated to this source.

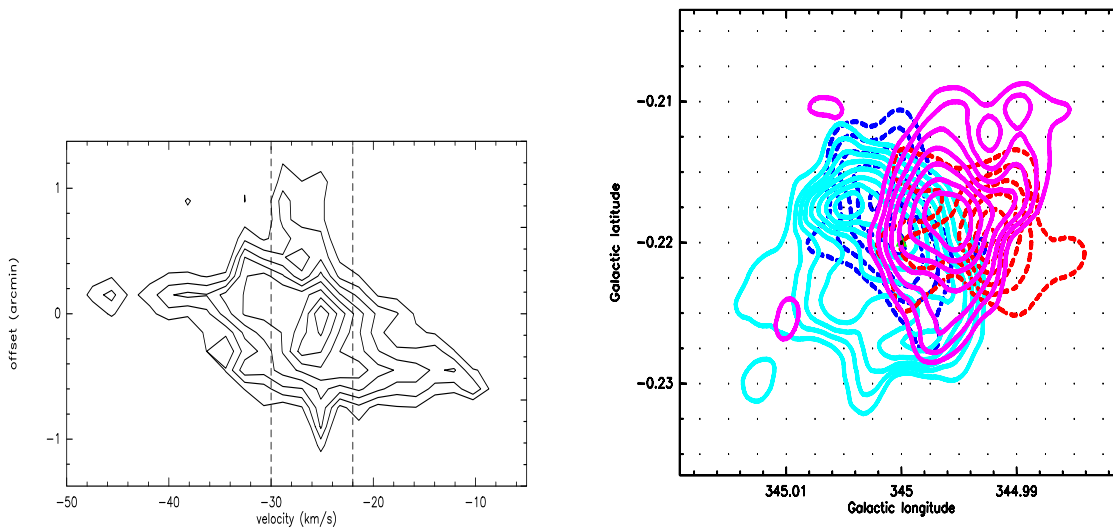


**Figure 7.** Left: SiO PV diagram of G345.0034-00.2240 cut along east-west direction. Contour levels are 30%, 40%...90% of the peak emission. Right: Outflow traced by SiO (dashed red and blue contours) superimposed with HNC<sup>+</sup> wing emissions (cyan and pink contours).

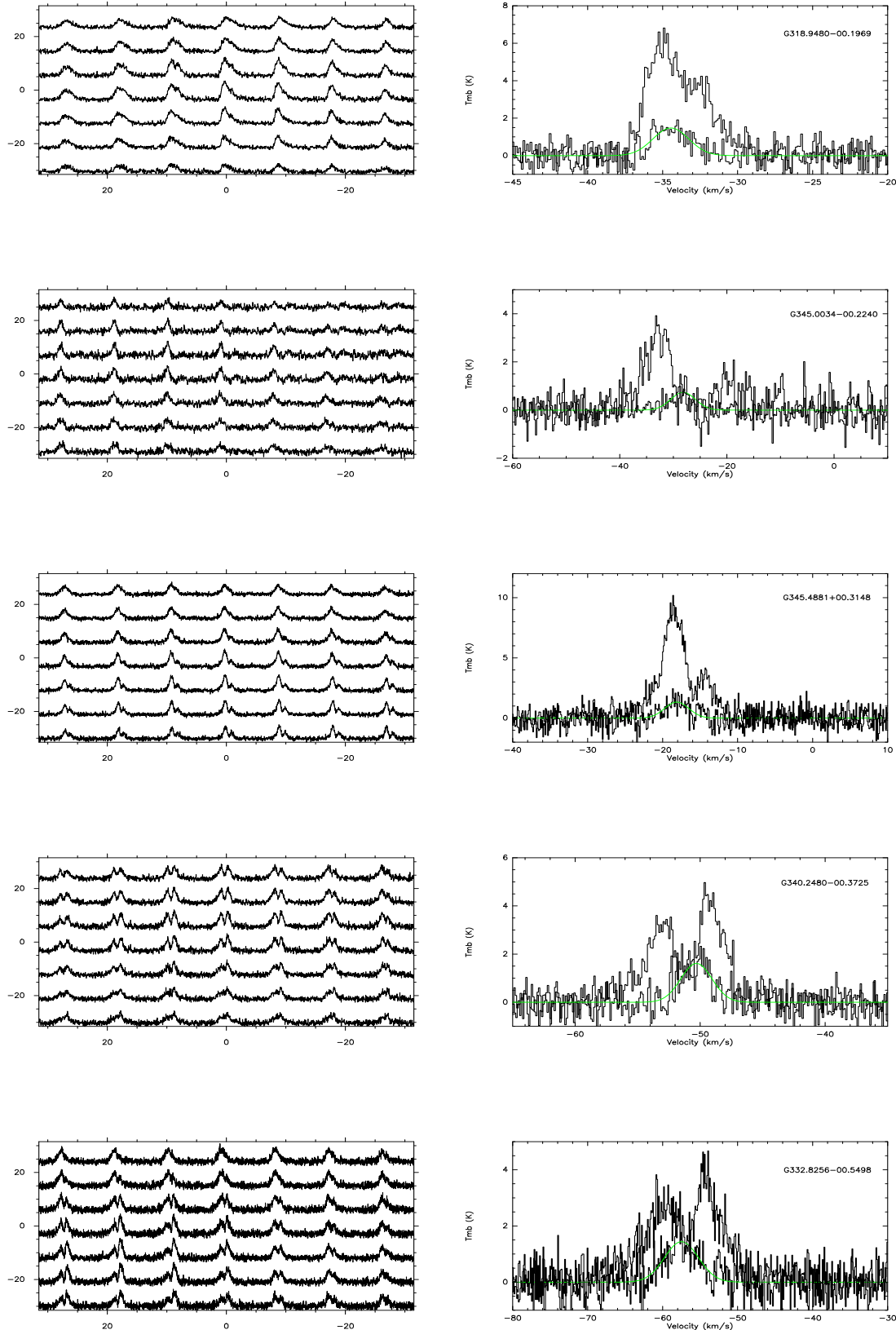


**Figure 8.** From the top and bottom panels present G318.9480-00.1969, G345.0034-00.2240, G345.4881+00.3148, G340.2480-00.3725 and G332.8256-00.5498  $\text{HCO}^+$  mapping observations (left) and its central spectra of  $\text{HCO}^+$  and  $\text{H}^{13}\text{CO}^+$  (right). The green lines are the  $\text{H}^{13}\text{CO}^+$  Gaussian-fitted lines.

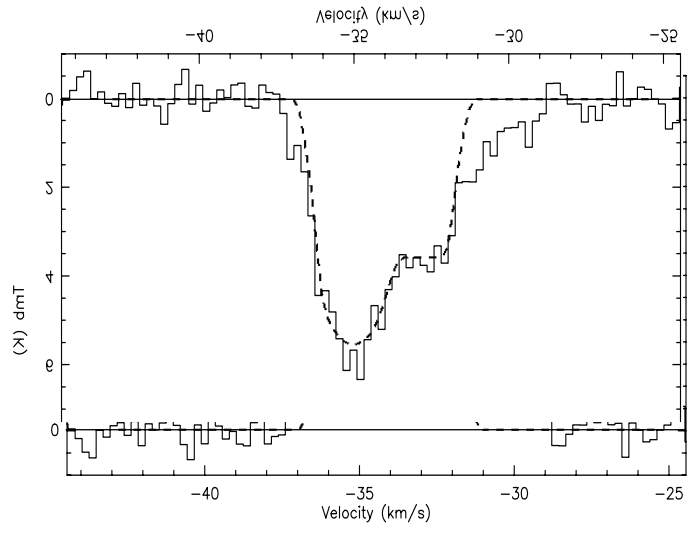


**Figure 9.** A comparison of the observed (solid) and model (dashed) HCO<sup>+</sup> spectra of G318.9480-00.1969.

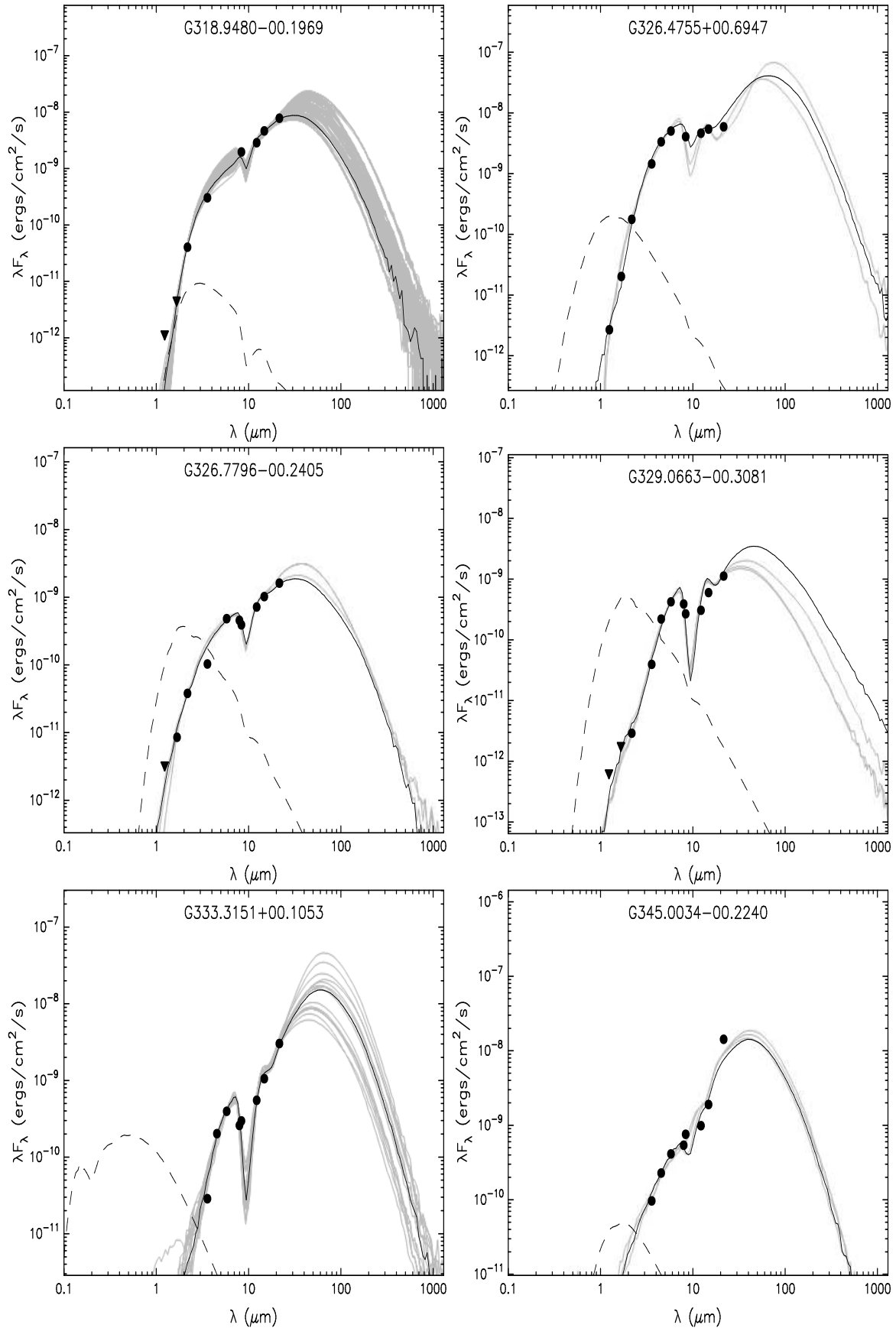


**Figure 10.** The SED fitting models. The dashed line represents the stellar photosphere model. The black line represents the best-fitting SED, and the gray lines represent all the other acceptable YSO fits.

# Molecular line study of massive star forming regions from the RMS survey

Naiping Yu<sup>1,2,3\*</sup> and Jun-Jie Wang<sup>1,2\*†</sup>

<sup>1</sup>National Astronomical Observatories, Chinese Academy of Sciences, Beijing 100012, China

<sup>2</sup>NAOC-TU Joint Center for Astrophysics, Lhasa 850000, China

<sup>3</sup>Graduate School of the Chinese Academy of Sciences, Beijing 100080, China

Accepted 20\*\* December 15. Received 20\*\* December 14

## ABSTRACT

In this paper we selected a sample of massive star forming regions from the Red MSX Source (RMS) survey, to study star formation activities (mainly outflow and inflow signatures). We focused on three molecular lines from the Millimeter Astronomy Legacy Team Survey at 90 GHz (MALT90): HCO<sup>+</sup>(1-0), H<sup>13</sup>CO<sup>+</sup>(1-0) and SiO(2-1). According to previous observations, our sources could be divided into two groups: nine massive young stellar object (MYSO) candidates (radio-quiet) and ten HII regions (having spherical or unresolved radio emissions). Outflow activities were found in eleven sources while only three show inflow signatures in all. The high outflow detection rate means outflows are common in massive star forming regions. The inflow detection rate was relatively low. We suggest this was due to beam dilution of the telescope. All the three inflow candidates have outflow(s). The outward radiation and thermal pressure from the central massive star(s) do not seem to strong enough to halt accretion in G345.0034-00.2240. Our simple model of G318.9480-00.1969 shows it has an infall velocity of about 1.8 km s<sup>-1</sup>. The spectral energy distribution (SED) analysis agrees our sources are massive and intermediate-massive star formation regions.

**Key words:** ISM: molecules - ISM: outflows and inflow - ISM: structure - stars: formation - stars: protostars

## 1 INTRODUCTION

Massive stars have a deep impact on the evolution of galaxies. Despite of their short lives, they determine the main chemical and physical properties of the nearby interstellar medium (ISM). Both theories and observations demonstrate they could hamper or trigger the next generation of star formation, by the expansion of HII regions and supernova explosions at the end of their lives (e.g. Elmegreen & Lada 1977; Lefloch & Lazareff 1994). However, their formation mechanism is still poorly understood as they used to form in clusters, and detail study of massive star formation is further hampered by their short lives, far distances, rare sources and extensive dust extinctions. Several mechanisms have been proposed that high-mass stars could form by accretion through massive disks (e.g. Keto et al. 2002), competitive accretions in dense clusters (Bonnell et al. 2004), ionized accretion (Keto & Wood, 2006), and mergers of several low-mass stars (Bonnell et al. 1998). The former three models are similar to that of low-mass star formation, accompanied by outflow during the process of gravitational collapse. Recent observations appear to favor the former three mechanism as stellar mergers require a high stellar density of  $\geq 10^8$  stars

pc<sup>-3</sup>, which is more than 4 orders of magnitude larger than those found in young embedded dense clusters (Bonnell 2002). Given the accretion timescales in massive star-forming regions are much shorter than those in low mass star-forming regions, the inside nuclear burning of hydrogen takes place while massive stars are still accreting, which means there is no pre-main-sequence stage for massive stars. Then substantial UV photons and ionized stellar winds rapidly ionize the surrounding hydrogen, forming a hypercompact HII region (HCHII) or ultracompact HII region (UCHII). Many questions are still unclear: whether accretion could be halted by the strong outward radiation and thermal pressure. Does it continue in an ionized form? Does it continue through a molecular or ionized disk?

In recent years, using color selection criteria and the IRAS point source catalogue, several attempts have been taken to search for MYSOs (e.g. Molinari et al. 1996; Sridharan et al. 2002). However, because of the large IRAS beam ( $\sim 3\text{-}5'$  at 100  $\mu\text{m}$ ), these selected samples tend to be biased towards bright, isolated sources and avoid dense clustered environments at the Galactic mid-plane. By comparing the the colors of sources from the MSX and 2MASS point sources to those known MYSOs, Lumsden et al. (2002) identified approximately 2000 MYSO candidates. The Red MSX Source (RMS) survey is an ongoing multi-wavelength observational programme and will provide us the largest MYSO sample

\* E-mail: yunaiping09@mails.gucas.ac.cn

†

**Table 1.** List of our sources

MSX name	RA (J2000)	Dec. (J2000)	Type (candidate)	$V_{lsr}^a$ (km s <sup>-1</sup> )	$D^a$ (kpc)	H <sub>2</sub> O maser
G316.5871-00.8086	14:46:23.24	-60:35:47.0	MYSO	-45.8	3.2	Y
G318.9480-00.1969	15:00:55.31	-58:58:52.6	MYSO	-34.5	2.6	Y
G326.4755+00.6947	15:43:18.94	-54:07:35.4	MYSO	-41.6	1.8	Y
G326.5437+00.1684	15:45:53.26	-54:30:01.3	MYSO	-74.1	3.6	N
G326.6618+00.5207	15:45:02.84	-54:09:03.0	MYSO	-39.1	1.8	Y
G326.7796-00.2405	15:48:55.20	-54:40:37.7	MYSO	-64.7	3.6	Y
G329.0663-00.3081	16:01:09.93	-53:16:02.3	MYSO	-42.6	2.9	Y
G333.3151+00.1053	16:19:29.00	-50:04:40.9	MYSO	-47.4	4.0	Y
G345.5043+00.3480	17:04:22.87	-40:44:23.5	MYSO	-17.8	2.1	Y
G327.9018+00.1538	15:53:10.87	-53:39:58.1	HII	-93.1	5.8	N
G329.3371+00.1469	16:00:33.13	-52:44:47.1	HII	-107.1	7.3	Y
G332.8256-00.5498	16:20:10.46	-50:53:28.6	HII	-4.0	0.19	N
G336.9842-00.1835	16:36:12.42	-47:37:57.5	HII	-75.1	10.8	Y
G337.0047+00.3226	16:34:04.73	-47:16:29.2	HII	-62.8	10.8	N
G339.1052+00.1490	16:42:59.58	-45:49:43.6	HII	-78.2	4.9	N
G340.2480-00.3725	16:49:29.97	-45:17:44.4	HII	-50.3	3.9	N
G345.0034-00.2240	17:05:11.19	-41:29:06.3	HII	-28.7	2.9	N
G345.4881+00.3148	17:04:28.04	-40:46:23.3	HII	-17.6	2.1	N
G348.8922-00.1787	17:17:00.10	-38:19:26.4	HII	1.0	18.2	Y

a: Urquhart et al. (2007b; 2008)

for statistical studies. Using the Australia Telescope Compact Array (ATCA), Urquhart et al. (2007a) completed the 5 GHz observations of 892 RMS sources in the southern sky. This programme divided these sources into three groups: real MYSO candidates, HII regions (UCHII and HCHII) and others such as evolved stars and planetary nebulae (PNe). To obtain kinematic distances, Urquhart et al. (2007b; 2008) made <sup>13</sup>CO (1-0) and (2-1) observations at Mopra, Onsala and Purple Mountain Observatory (PMO) 13.7 m telescope, and the 15 m James Clerk Maxwell Telescope (JCMT), as well as archival data extracted from the Galactic Ring Survey (GRS). They found that the majority of these sources have multiple velocity components along each line of sight. The multiple emission features make it difficult to assign a unique kinematic velocity to each source. In order to identify a more reliable molecular component, they further searched archival water and methanol masers catalogues of Valdetarro et al. (2001) and Pestalozzi et al. (2005), less abundant but denser gas molecular traces like CS (2-1) observations by Bronfman et al. (1996). And then by using the rotation curve of Brand and Blitz (1993) and their radial velocities, kinematic distances for all detected components can be derived. Based on the above observations and research, we selected about twenty RMS sources to study star formation activities (mainly outflow and inflow signatures) using data from Millimeter Astronomy Legacy Team 90 GHz survey (MALT90). We present the introductions of our data and source selections in section 2, results and analysis in section 3, and summary in section 4.

## 2 DATA AND SOURCE SELECTIONS

The MALT90 is a large international project aimed at characterizing the sites within our Galaxy where high-mass stars will form. Exploiting the unique broad frequency range and fast-mapping capabilities of the Mopra 22-m telescope, MALT90 maps 16 emission lines simultaneously at frequencies near 90 GHz. These molecular lines will probe the physical, chemical, and evolutionary states of

dense high-mass star-forming cores. We focused on three molecular lines from the MALT90 Survey: HCO<sup>+</sup>(1-0), H<sup>13</sup>CO<sup>+</sup>(1-0) and SiO(2-1). HCO<sup>+</sup> often shows infall signatures and outflow wings (e.g., Rawlings et al. 2004; Fuller et al. 2005). H<sup>13</sup>CO<sup>+</sup>(1-0) provides optical depth and line profile information. SiO (2-1) is seen when SiO is formed from shocked dust grains, typically in outflows (Schilke et al. 1997). The survey covers a Galactic longitude range of  $\sim -60$  to  $\sim 15^\circ$  and Galactic latitude range of  $-1$  to  $+1^\circ$ . The observations were carried out with the newly upgraded Mopra Spectrometer (MOPS). The full 8 GHz bandwidth of MOPS was split into 16 zoom bands of 138 MHz each providing a velocity resolution of  $\sim 0.11$  km s<sup>-1</sup>. The angular resolution of Mopra is about 38 arcsec, with beam efficiency between 0.49 at 86 GHz and 0.42 at 115 GHz (Ladd et al. 2005). The maps were made with 9'' spacing between adjacent rows. More information about this survey can be found in Foster et al. (2011) and Hoq et al. (2013). The MALT90 data includes ( $l, b, v$ ) data cubes and ( $l, b$ ) moment and error maps, and is publicly available from the MALT90 Home Page<sup>1</sup>. The data processing was conducted using CLASS (Continuum and Line Analysis Single-Disk Software) and GreG (Grenoble Graphic) software packages.

In order to study massive star formation activities (mainly outflow and inflow signatures), we selected nineteen sources from the RMS survey by applying the following criteria: (1) Sources should not be on the edge of known HII or supernova regions, considering the large beam of the 22 m Mopra telescope; (2) According to the observations of ATCA (Urquhart et al. 2007a), sources should be radio quiet or have a simple spherical/unresolved radio emissions; (3) All sources should be detected by MALT90; (4) The LSR velocities of HCO<sup>+</sup> and H<sup>13</sup>CO<sup>+</sup> should be the same as Urquhart et al. (2007b; 2008). We need to mention here that our sample is not complete according to the above four criteria. We wish a much more complete research of the RMS sources by the MALT90 data in the

<sup>1</sup> See <http://atoa.atnf.csiro.au/MALT90>



**Table 2.** Outflow parameters

Source	Shift	$\Delta v$ (Km s <sup>-1</sup> )	N (HCO <sup>+</sup> ) ( $\times 10^{12}$ cm <sup>-2</sup> )	M (M <sub>⊙</sub> )	P <sub>out</sub> (M <sub>⊙</sub> km s <sup>-1</sup> )	E <sub>out</sub> (M <sub>⊙</sub> [km s <sup>-1</sup> ] <sup>2</sup> )
G326.4755+00.6947	red	(-40, -33)	22.4	16.8	118	412
	blue	(-47, -42)	17.7	19.0	95	238
G326.7796-00.2405	red	(-64, -62)	10.0	21.4	43	43
	blue	(-69, -66)	8.91	23.9	72	108
G333.3151+00.1053	red	(-45.3, -44)	4.8	15.2	20	13
	blue	(-50, -47)	11.8	46.8	140	211
G345.5043+00.3480	red	(-12, -15)	12.2	6.7	20	30
	blue	(-20, -24)	9.1	10.0	40	80
G329.3371+00.1469	red	(-106, -104)	8.9	78.4	157	157
	blue	(-112, -110)	5.6	49.3	99	99
G332.8256-00.5498	red	(-49, -53)	14.0	1.0	4	8
	blue	(-65, -61)	11.3	1.7	7	14
G340.2480-00.3725	red	(-49, -46)	9.5	50.2	151	226
	blue	(-56, -53)	10.7	65.9	198	297
G345.0034-00.2240 <sup>a</sup>	red	(-22, -19)	6.1	14.8	89	266
	blue	(-35, -31)	9.8	28.6	172	515
G345.4881+00.3148	red	(-15, -12)	14.0	21.6	65	97
	blue	(-22, -19)	21.8	28.6	86	129

a: The outflow parameters of this source are calculated by HNC(1-0).

near future. The information of our selected sources are listed in table 1. Nearly all of the MYSO candidates are associated with water masers according to former observations, however in the HII regions only three sources are associated with water maser emissions. This suggests in massive star formation regions, water masers are more likely to be associated with MYSOs than HII regions.

### 3 RESULTS AND DISCUSSIONS

Infall and outflow are two of the most important elements to understand the theories of massive star formation. Infall can act to replenish disk material as mass falls onto a protostar, while outflows serve as a release mechanism for the angular momentum that builds up during the accretion process. These motions can be studied by investigating the profiles of optically thick and optically thin molecular lines. Blue profile, a combination of a double peak with a brighter blue peak or a skewed single blue peak in optically thick lines, can be used to study infall motions (Sun et al. 2008). Surely blue profile may also be caused by rotation and outflow. However, infall motion is the only process that would produce consistently the blue profile. Outflow and rotation only produce a blue asymmetric line profile along a particular line of sight to a source (Sun et al. 2008).

SiO is also a well-known tracer of recent outflow. In the cold diffuse ISM, the element of Si is regarded to be frozen into dust grains. When the gas is shocked (i.e., the gas through which a protostellar outflow is passing) the dust grains can sublimate and Si is released into gas phase. Thus, the detections of SiO emissions from MYSOs could always be equal to the detections of recent outflow activities. In the following sections, we use position-velocity (PV) diagram of HCO<sup>+</sup> (1-0) and/or SiO (2-1) (if detected) to study outflows in our sample. For G318.9480-00.1969, we also employed

the three dimensional radiative-transfer code RADMC3D, developed by C. Dullemond<sup>2</sup>, to compute the HCO<sup>+</sup> (1-0) line emission from an infalling model.

#### 3.1 Outflow signatures detected by HCO<sup>+</sup> (1-0) and SiO (2-1)

Outflow makes an important contribution to the line wing emissions of HCO<sup>+</sup> (1-0), as it becomes optically thick quickly and readily self-absorbs in dense gas regions. We drew PV diagrams for our sources. According to the PV diagrams, we selected the integrated range of wings and determined the outflow intensities of red and blue lobes. Four HCO<sup>+</sup> (1-0) PV diagrams of our nine MYSO candidates and four in ten HII regions show distinct wing emissions (figure 1 and figure 2, respectively), which may be probably caused by bipolar outflows. Figure 3 and figure 4 show the integrated maps by integrating wing emissions of our MYSOs and HII regions, respectively. The Mopra beam size is 38'' and the spacing of the spectra is 9'', so there are about  $4 \times 4 = 16$  spectra within a single beam. In the sample of MYSOs, the peak emissions of red and blue lobes are within one beam and we could not determine the outflow directions. It also seems impossible that all the axis of these outflows are nearly parallel with the line of sight. By comparing figure 3 and figure 4, it can be noted that the MYSO outflows are more compact than those found in HII regions. Considering the mean distance of our RMS sources with radio emission ( $\sim 5.7$  kpc) is larger than those radio quiet ( $\sim 2.6$  kpc), our result agrees MYSO candidates should be in much earlier stage than HCHII/UCHII regions.

Figure 5 shows the five detected SiO spectra toward our sources. Among these five sources, three (G318.9480-00.1969, G326.4755+00.6947, G329.0663-00.3081) are MYSO candidates

<sup>2</sup> See <http://www.ita.uni-heidelberg.de/dullemond/software/radmc-3d/>

**Table 3.** SED parameters

RMS sources	Stellar mass [M <sub>⊙</sub> ]	Disk mass [M <sub>⊙</sub> ]	Envelope mass [M <sub>⊙</sub> ]	Total luminosity [L <sub>⊙</sub> ]	Best-fit model
G318.9480-00.1969	9.56	$4.68 \times 10^{-3}$	$9.65 \times 10^0$	$5.72 \times 10^3$	3014991
G326.4755+00.6947	10.10	$9.77 \times 10^{-3}$	$1.14 \times 10^3$	$9.06 \times 10^3$	3000136
G326.7796-00.2405	8.08	$4.58 \times 10^{-2}$	$2.68 \times 10^1$	$7.33 \times 10^2$	3004818
G329.0663-00.3081	9.49	$5.52 \times 10^{-2}$	$3.08 \times 10^1$	$1.45 \times 10^3$	3010080
G333.3151+00.1053	13.91	$5.88 \times 10^{-4}$	$6.46 \times 10^2$	$1.70 \times 10^4$	3000244
G345.0034-00.2240	9.67	$7.58 \times 10^{-2}$	$4.42 \times 10^1$	$7.81 \times 10^3$	3003254

and the other two (G340.2480-00.3725 and G345.0034-00.2240) are HII regions. Models and observations also suggest SiO emissions could be caused by photodissociated region (PDR) and not an outflow (e.g. Schilke et al. 2001; Shepherd et al. 2004). For the MYSO candidates, as they are radio quiet, SiO emissions triggered by PDR around HII regions are impossible. However, a PDR could also exist without the presence of ionized gas. Through the method described by Klaassen et al. (2007), we estimated the SiO column densities  $> 10^{14} \text{ cm}^{-2}$  of the five sources, much larger than those found in PDRs ( $\sim 10^{12} \text{ cm}^{-2}$ ) (Schilke et al. 2001). We thus regard these SiO emissions are due to recent outflow activities.

We should mention that the outflow detection rate is just a low limit. One reason is due to the beam dilution, especially for the MYSO candidates. For example outflow activity was not found in MYSO G318.9480-00.1969 through PV diagram analysis, however the SiO emission discussed above shows recent outflow(s) in this region. Outflow(s) in this source may be very young and is thus heavily diluted. The other reason is due to the molecular line we used to trace outflow. Considering the wide range of physical conditions in star formation regions (i.e. gas densities from  $\sim 10^{-20} \text{ g cm}^{-3}$  to  $\sim 10^{-16} \text{ g cm}^{-3}$ , and gas temperatures from  $\sim 10 \text{ K}$  to  $\sim 100 \text{ K}$ ), there is non-trivial molecular tracer to detect outflows in all conditions. For example, the PV diagram of HCO<sup>+</sup> in G345.0034-00.2240 does not show red-shifted emission wings (figure 6). The gas near -17 km/s is possibly unrelated to this source. However, when we chose HNC instead of HCO<sup>+</sup>, wing emissions caused by bipolar outflow was evident. Besides, the SiO spectra of G345.0034-00.2240 extends from -8 km s<sup>-1</sup> to -48 km s<sup>-1</sup>. The wide line emissions further suggest young outflow activities. PV diagram of SiO in G345.0034-00.2240 cut along east-west direction is shown in figure 7. Figure 7 also shows the maps of the integrated blue and red shifted SiO (2-1) emission (the dash contours). It can be noted SiO traces the inner region of the outflow, compared to HNC. The outflow detection rate by SiO in MYSOs ( $\sim 33 \%$ ) is much higher than that in HII regions ( $\sim 20 \%$ ). That is because SiO is particularly well suited to tracing recent outflows, as it persists in the gas phase for only  $\sim 10^4$  years after being released by shocks (e.g., Pineau des Forets et al. 1997).

Assuming that HCO<sup>+</sup> (1-0) emission in the line wings to be optically thin and Local Thermodynamic Equilibrium (LTE),  $X(\text{HCO}^+) = [\text{HCO}^+]/[\text{H}_2] = 10^{-8}$  (Turner et al. 1997) and  $T_{ex} = 15 \text{ K}$ , we derive the column density using:

$$N(\text{HCO}^+) = Q(T_{ex}) \frac{8\pi\nu_0^3}{c^3} \frac{g_l}{g_u A_{ul}} \frac{1}{[1 - e^{-h\nu_0/kT_{ex}}]^{-1}} \int \tau dv \quad (1)$$

where  $\nu_0$ ,  $g_u$ ,  $g_l$  and  $A_{ul}$  are the rest frequency, the upper and lower level degeneracies and the Einstein's coefficient of HCO<sup>+</sup>,  $Q(T_{ex})$  is the partition function, and  $c$  is the speed of light. In addition,

by assuming that the HCO<sup>+</sup> emission is optically thin in the line wings, we use the approximation:

$$\int \tau dv = \frac{1}{J(T_{ex}) - J(T_{bg})} \int T_{mb} dv \quad (2)$$

where  $T_{bg}$  is the temperature of the background radiation (2.73 K). Using  $M_{out} = \mu m_H d^2 \Omega X(\text{HCO}^+)^{-1} N(\text{HCO}^+)$ , we obtain the masses for the red and blue molecular outflows, where  $N(\text{HCO}^+)$  is the HCO<sup>+</sup> column density calculated through the above equations,  $d$  is the distance,  $\Omega$  is the area of the lobes (within 50% of each peak emission), and  $m_H$  is the hydrogen atom mass. We adopt a mean molecular weight per H<sub>2</sub> molecule of  $\mu = 2.72$  to include helium. We estimate the momentum and energy of the red and blue lobes using

$$P_{out} = M_{out} V \quad (3)$$

and

$$E_{out} = \frac{1}{2} M_{out} V^2 \quad (4)$$

where  $V$  is a characteristic velocity estimated as the difference between the maximum velocity of HCO<sup>+</sup> emission in the red and blue wings respectively, and the molecular ambient velocity ( $V_{lsr}$ ). The derived parameters are shown in table 2.

## 3.2 Infall

### 3.2.1 The blue profile

Previous studies show HCO<sup>+</sup> (1-0) is a good inward motion tracer in star formation regions (e.g. Sun et al. 2008). The five HCO<sup>+</sup> (1-0) emission lines of our sources (figure 8, right panels) are far of having a simple Gaussian shape, presenting asymmetries, and spectral wings or shoulders, which suggest that the molecular gas is affected by the dynamics of these star-forming regions. However, we know double peak could also be caused by two velocity components in the line of sight. The detections of optically thin molecular lines such as H<sup>13</sup>CO<sup>+</sup> (1-0) could help us to rule out this possibility. Mapping observations could help us to identify whether this was caused by inward motions or other dynamics such as outflow, rotation and expansions of HII regions. Figure 8 (the left panels) shows the mapping observations towards our sources with double peaked HCO<sup>+</sup> (1-0) emissions. All the spectra of H<sup>13</sup>CO<sup>+</sup> in figure 8 peaks near the dip of HCO<sup>+</sup>. Besides, three of them (G318.9480-00.1969, G345.0034-00.2240 and G345.4881+00.3148) show consistent blue profiles, indicating infall motions. To quantify the blue profile, we further used the asymmetry parameter  $\delta V$  defined as the difference between the peak velocities of an optically thick line  $V(\text{thick})$  and an optically thin line  $V(\text{thin})$  in units of the optically thin line FWHM (Full Width at Half Maximum)  $dV(\text{thin})$ :  $\delta V =$

$\frac{V(\text{thick})-V(\text{thin})}{dV(\text{thin})}$ . Mardones et al. (1997) adopted a criterion  $\delta V < -0.25$  to indicate blue asymmetry. Our calculations further demonstrate blue profiles caused by inflow in G318.9480-00.1969 ( $\delta V = -0.27$ ), G345.0034-00.2240 ( $\delta V = -0.63$ ) and G345.4881+00.3148 ( $\delta V = -0.37$ ). Outflow activities are also detected in these regions (see section 3.1). This suggests that like low star formation theories, massive stars in these regions are probably forming through accretion-outflow process. For G345.0034-00.2240, if the detection of recent outflow activity traced by SiO and the appearance to be undergoing infall are indeed caused by the central massive young star(s), this suggests the outward radiation and thermal pressure from the central massive star(s) do not strong enough to halt accretion. Like the case of G10.6-0.4 (Keto & Wood 2006), accretion flow in this region may be ionized. Given the low angular resolution of the data (at 2.9 kpc,  $38''$  is over half a parsec), it is also possible that a lower mass star is forming in the vicinity. Deeper observations should be carried out to study our speculation.

Sun et al. (2008) made single-pointing and mapping observations of  $\text{HCO}^+$  (1-0) from the 13.7m telescope of PMO. Among their 29 massive star-forming cores (mainly UCHII regions), six sources were identified to be strong infall candidates. The detection rate is consistent with our study, even though the resolution of Mopra is much higher than that of the 13.7m telescope ( $38''$  vs.  $58''$ ). This may be because all of their source distances are less than 4 kpc while half of our sources locate more than 5 kpc away. Klaassen et al. (2007,2012) also obtained JCMT observations of  $\text{HCO}^+/\text{H}^{13}\text{CO}^+$  (4-3) to trace large scale inward motions in a sample of massive star-forming regions (mainly MYSOs, HCHII and UCHII regions). The infall rate in our sample is relatively low compared with their work. This partly may be due to their higher resolution ( $15''$  vs.  $38''$ ). Besides, the  $J = 4-3$  transition is likely a better asymmetry tracer than  $J = 1-0$  (see figure 8 of Tsamis et al. 2008). Only one source in our MYSO candidates shows infall signature. This may be because the infall area within MYSO is relatively smaller than that in UCHII regions, and then more likely to be beam diluted.

### 3.2.2 A simple infall model of G318.9480-00.1969

G318.9480-00.1969 is the only MYSO candidate showing infall signature. In this section, in order to constrain the spatial and dynamic structures of G318.9480-00.1969, we constructed a radiative-transfer model that reproduces the observations. The three-dimensional radiative-transfer code RADMC-3D, developed by C. Dullemond, was employed to compute the dust temperature from stellar heating and the continuum and line emission of an infall model. The dust opacity is from Ossenkopf & Henning (1994) without grain mantles or coagulation. The molecular data of  $\text{HCO}^+$  comes from the Leiden LAMDA database<sup>3</sup>. The line transfer assumes the gas temperature to be equal to the dust temperature and LTE (full non-LTE radiation transfer is also planned for RADMC-3D).

In our model, the volume density follows a radial power law,  $n \propto r^{-1.5}$ , with a total mass of  $31 M_{\odot}$  (estimated from our observations) within a box of  $(4000 \text{ AU})^3$ . Inside there is a star of  $10 M_{\odot}$  (see section 3.3). The gas has a turbulence velocity of  $0.5 \text{ km s}^{-1}$  and is radially infalling with  $1.8 \text{ km s}^{-1}$  to the central star. The model is inevitably simplified. A comparison of the observed and

model spectra is shown in figure 9. At the center, the model spectra matches well with the observation. However, the observed line seems to have line wing emissions, probably caused by outflow activities. The detected SiO spectra in this region indeed implies beam diluted outflow(s). Even though our model is consistent with the data, we should realize it does not provide errors of the parameters, and different models may also fit as well. However, it provides us a way to study the structure of star forming regions.

### 3.3 Spectral energy distribution

In this section, we try to fit the spectral energy distribution (SED) of our sources using the tool developed by Robitaille et al. (2007). Briefly, the SED-fitting tool works as a regression method to find the SEDs within a specified  $\chi^2$  from a large grid of models after fitting the input data points. The grid of models contains stellar masses, disk masses, mass accretion rates, and line-of-sight (LOS) inclinations. The grid of YSO models was computed by Robitaille et al. (2006) using the 20,000 two-dimensional radiation transfer models from Whitney et al. (2003a, 2003b, 2004). Each YSO model has SEDs for 10 viewing angles (inclinations), so the total YSO grid consists of 200,000 SEDs. We use archival data from 2MASS, IRAC of Spitzer, MSX to fit the SED of our sources. In addition to the best-fit model (the black line in figure 10), we also show the range of possible parameters that can be derived from models within the range of  $\chi^2/\nu - \chi^2_{\text{best}}/\nu \leq 4$  ( $\nu$  represents the number of data points). The best derived model parameters are listed in table 3 and the resulting SEDs are shown in figure 10. Of these six sources, five are HII regions. This may be because the protostar(s) of MYSOs are still deeply imbedded, even infrared emissions are hard to be detected. The SED agrees our sources are massive and intermediate-massive star formation regions, with masses ranging from 8 to  $14 M_{\odot}$ .

## 4 SUMMARY

By analyzing  $\text{HCO}^+$ (1-0),  $\text{H}^{13}\text{CO}^+$ (1-0) and  $\text{SiO}$ (2-1) molecular data from MALT90, we studied the outflow and infall activities in nineteen RMS sources. The high outflow detection rate ( $\geq 58\%$ ) suggests that outflows are common in massive star forming regions as in low mass star forming regions. All of the detected outflows in our radio-quiet RMS sources are much more compact than those found in radio-loud RMS sources, indicating they are at earlier stages. The outward radiation and thermal pressure from the central massive star(s) of G345.0034-00.2240 do not seem to strong enough to halt accretion in this region. The detection of recent outflow activity traced by SiO and the appearance to be undergoing infall in this region suggest ionized accretion flow can continue through an HII region and massive star(s) in this region could be formed through ionized accretions. Only one source of our MYSO candidates shows infall signature. This may be because the infall area with MYSO is relatively small, and thus more likely to be beam diluted. A simple model of G318.9480-00.1969 shows it has an infall velocity of about  $1.8 \text{ km s}^{-1}$ . The spectral energy distribution (SED) further agrees our RMS sources are massive and intermediate-massive star formation regions.

<sup>3</sup> <http://www.strw.leidenuniv.nl/~moldata>

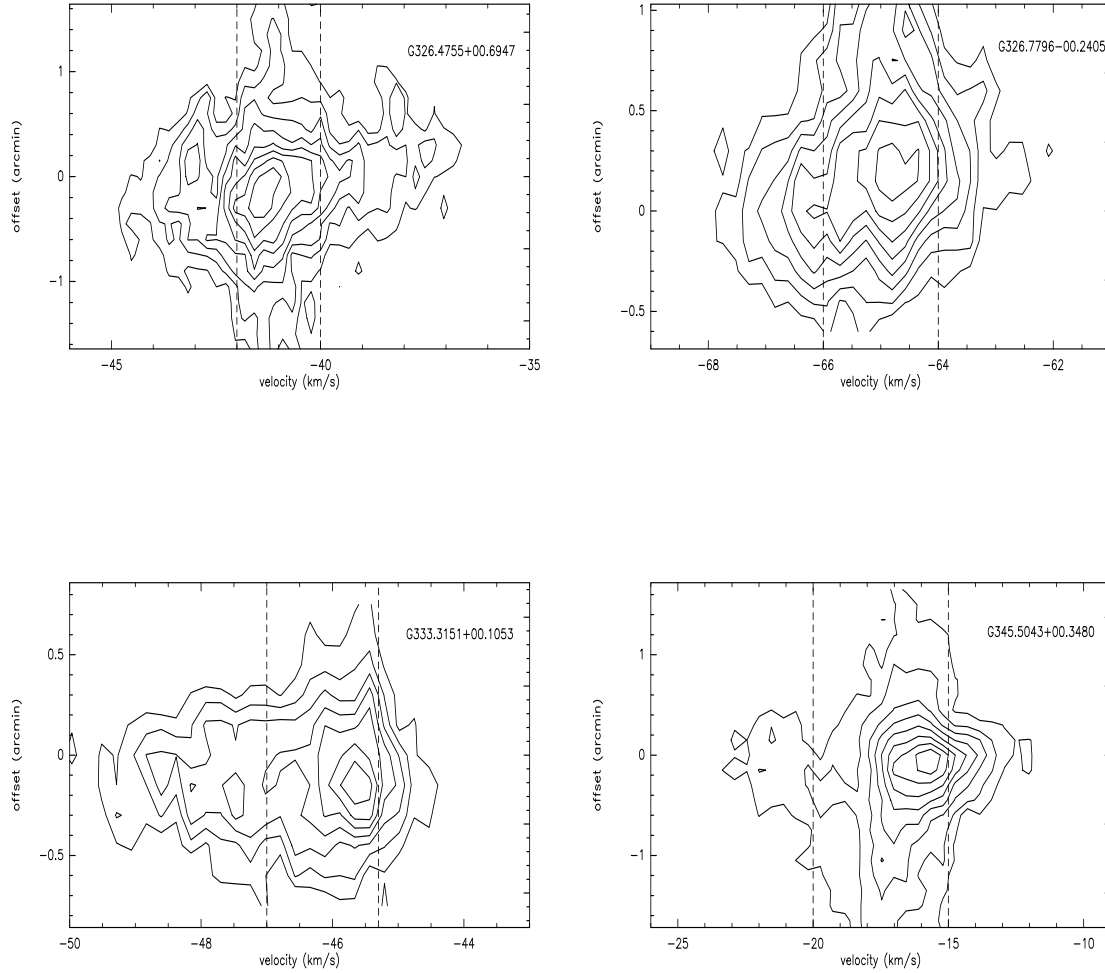


**Figure 1.** PV diagrams of the MYSO candidates show HCO<sup>+</sup> (1-0) wing emissions. Contours are 20%, 30%...90% of the peak emissions. The dashed lines indicate the velocity ranges for the blue and red wings as listed in table 2.

## 5 ACKNOWLEDGEMENTS

We thank the anonymous referee for constructive suggestions. This paper made use of information from the Red MSX Source (RMS) survey database [http://rms.leeds.ac.uk/cgi-bin/public/RMS\\_DATABASE.cgi](http://rms.leeds.ac.uk/cgi-bin/public/RMS_DATABASE.cgi) which was constructed with support from the Science and Technology Facilities Council of the UK. This research made use of data products from the Millimetre Astronomy Legacy Team 90 GHz (MALT90) survey. The Mopra telescope is part of the Australia Telescope and is funded by the Commonwealth of Australia for operation as National Facility managed by CSIRO.

## REFERENCES

- Bonnell, I.A. et al 1998, MNRAS, 298, 93  
 Bonnell, I.A. 2002, in ASP Conf.Ser. 267, The Earliest Stages of Massive Star Birth, ed. P.A. Crowther (San Francisco: ASP), 193

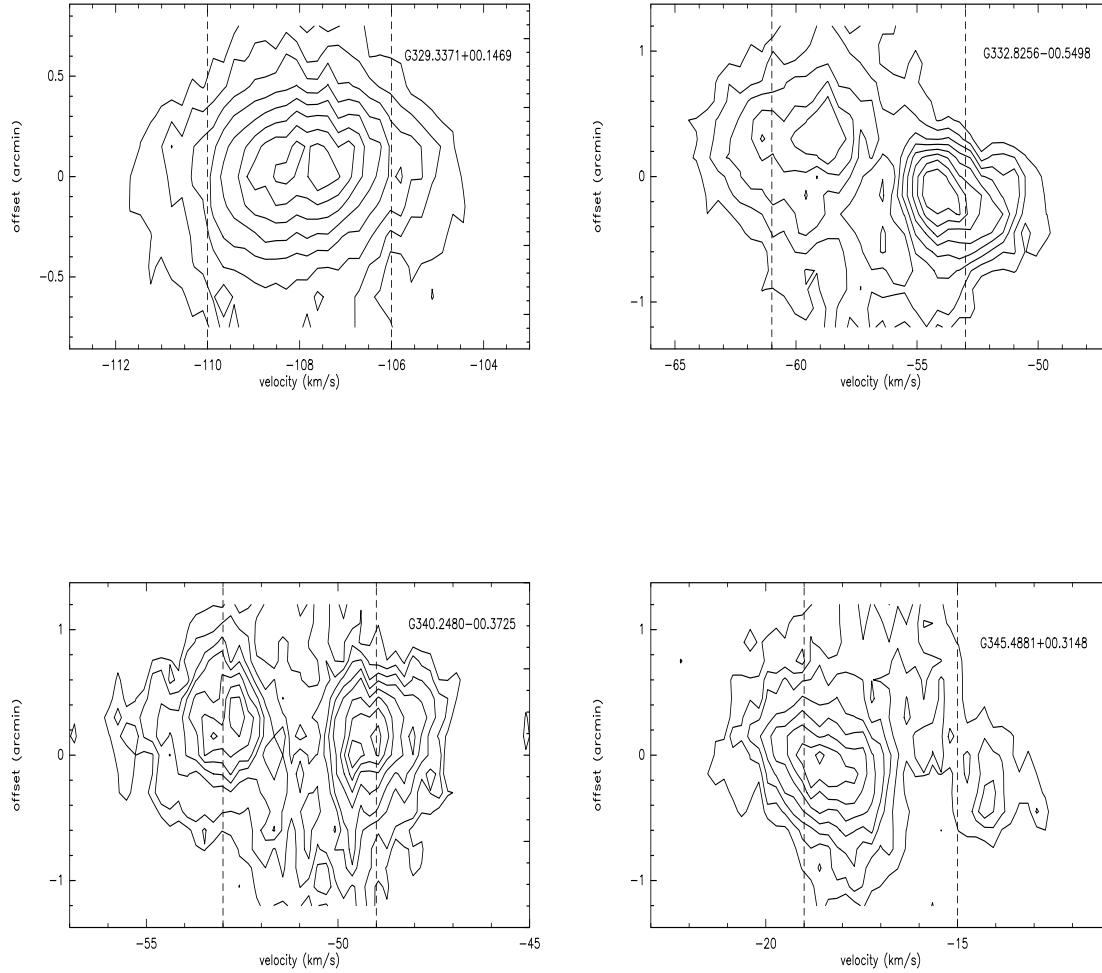


**Figure 2.** PV diagrams of the HII candidates show HCO<sup>+</sup> (1-0) wing emissions. Contours are 20%, 30%...90% of the peak emissions. The dashed lines indicate the velocity ranges for the blue and red wings as listed in table 2.

Bonnell, I.A. et al. 2004, MNRAS, 349, 735  
 Bronfman, L., Nyman, L.-A., May, J., 1996, A&AS, 115, 81  
 Elmegreen, B. G., Lada C.J., 1977, ApJ, 214, 725  
 Foster J.B., et al. 2011, ApJS, 197, 25  
 Fuller, G. A., Williams, S. J., Sridharan, T. K., 2005, A&A, 442, 949  
 Hoq, S., Jackson, J.M., Foster, J.B., et al. 2013, ApJ, 777, 157  
 Keto, E. 2002, ApJ, 580, 980  
 Keto, E., Wood, K. 2006, ApJ, 637, 850  
 Klaassen, P.D., Wilson, C.D., 2007, ApJ, 663, 1092  
 Klaassen, P.D., Testi, L., Beuther, H., 2012, A&A, 538, 140  
 Ladd, N., Purcell, C., Wong, T., & Robertson, S. 2005, PASA, 22, 62  
 Lefloch, B., Lazareff, B., 1994, A&A, 289, 559  
 Lumsden, S. L., Hoare, M. G., Oudmaijer, R. D., Richards, D. 2002, MNRAS, 336, 621  
 Mardones, D., Myers, P. C., Tafalla, M. et al. 1997, ApJ, 489, 719  
 Molinari, S., Brand, J., Cesaroni, R., Palla, F. 1996, A&A, 308, 573  
 Ossenkopf, V., & Henning, T. 1994, A&A, 291, 943  
 Pestalozzi, M.R., Minier, V., Booth, R.S., 2005, A&A, 432, 737

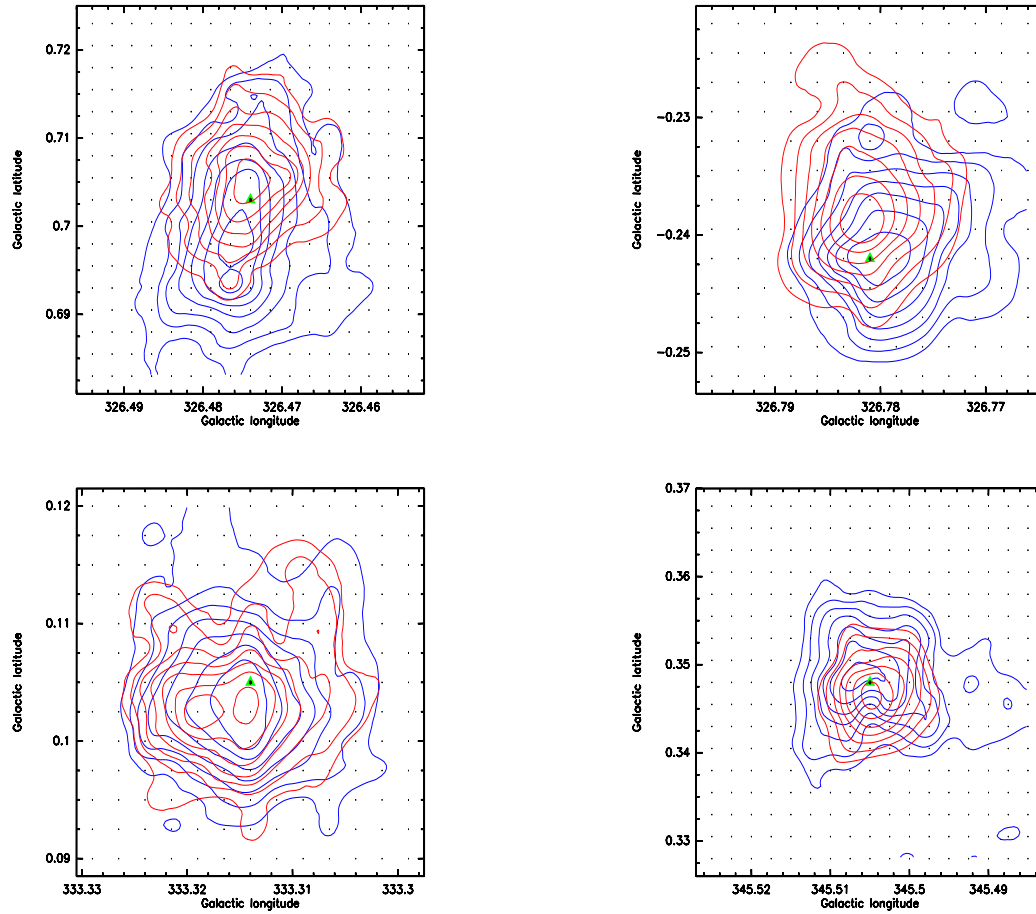


**Figure 3.** The blue and red contours show the  $\text{HCO}^+$  (1-0) integrated wing emissions of the MYSO candidates. The green triangles mark the RMS sources and the dot symbols mark the mapped points. The levels are 30%, 40%...90% of the peak emissions respectively.

- Pineau des Forets, G., Flower, D. R., & Chieze, J.-P. 1997, in IAU Symp. 182, Herbig-Haro Flows and the Birth of Stars, ed. B. Reipurth & C. Bertout (Dordrecht: Kluwer), 199
- Rawlings, J. M. C., Redman, M. P., Keto, E., Williams, D. A., 2004, MNRAS, 351, 1054
- Robitaille, T. P., Whitney, B. A., Indebetouw, R., Wood, K., Denzmore, P., 2006, ApJS, 167, 256
- Robitaille, T. P., Whitney, B. A., Indebetouw, R., Wood, K., 2007, ApJS, 169, 328
- Schilke, P., Walmsley, C. M., Pineau des Forets, G., Flower, D. R., 1997, A&A, 321, 293
- Schilke, P., Pineau des Forêts, G., Walmsley, C.M., et al., 2001, A&A, 372, 291
- Shepherd, D.S., Kurtz, S.E., Testi, L. 2004, ApJ, 601, 952
- Sridharan, T. K., Schilke, P., Menten, K. M., Wyrowski, F. 2002, ApJ, 566, 931
- Sun Yan, Gao Yu, 2009, MNRAS, 392, 170
- Tsamis, Y.G., Rawlings, J.M.C., Yates, J.A., Viti, S. 2008, MNRAS, 388, 898
- Urquhart, J. S., Busfield, A. L., Hoare, M. G., et al. 2007a, A&A, 461, 11
- Urquhart, J. S., et al. 2007b, A&A, 474, 891
- Urquhart, J. S., et al. 2008, A&A, 487, 253
- Valdettaro, R., Palla, F., Brand, J., et al. 2001, A&A, 368, 845
- Whitney, B. A., Indebetouw, R., Bjorkman, J.E., Wood, K., 2004, ApJ, 617, 1177
- Whitney, B. A., Wood, K., Bjorkman, J. E., Cohen, M., 2003a, ApJ, 598, 1079
- Whitney, B. A., Wood, K., Bjorkman, J. E., Wolff, M. J., 2003b, ApJ, 591, 1049

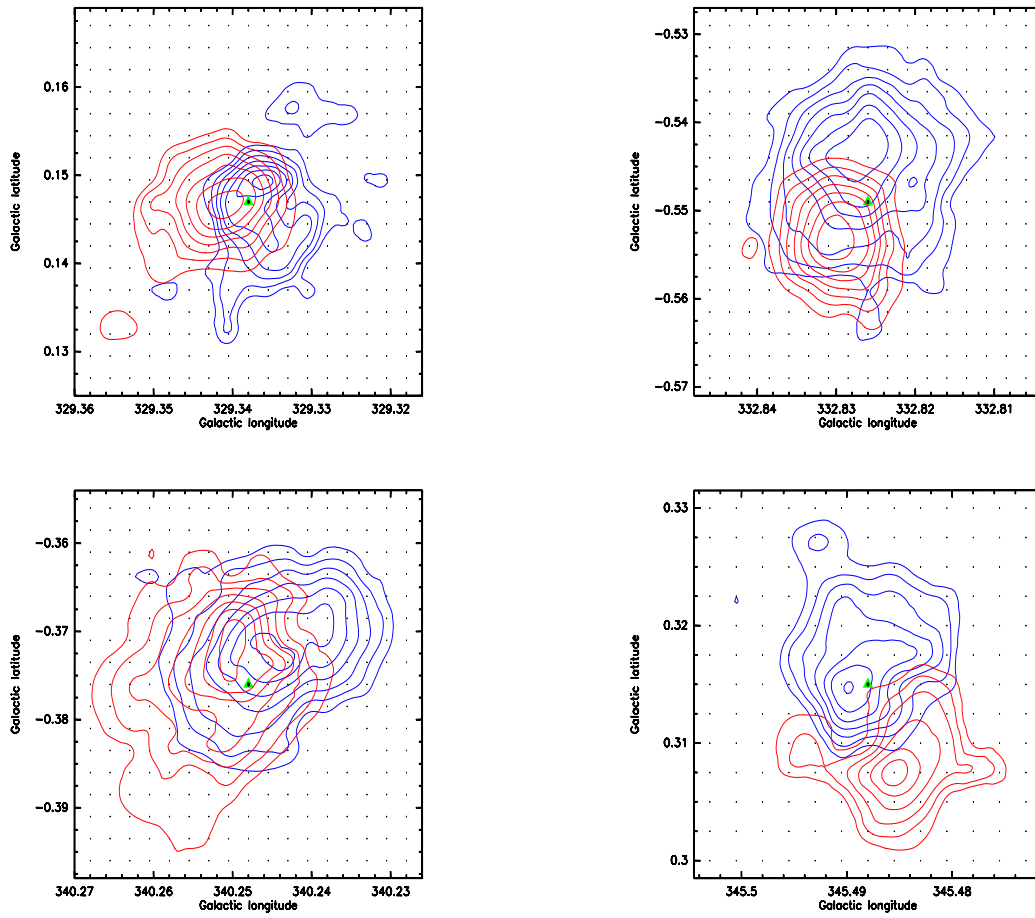


**Figure 4.** The blue and red contours show the HCO<sup>+</sup> (1-0) integrated wing emissions of the HII candidates. The green triangles mark the RMS sources and the dot symbols mark the mapped points. The levels are 30%, 40%...90% of the peak emissions respectively.

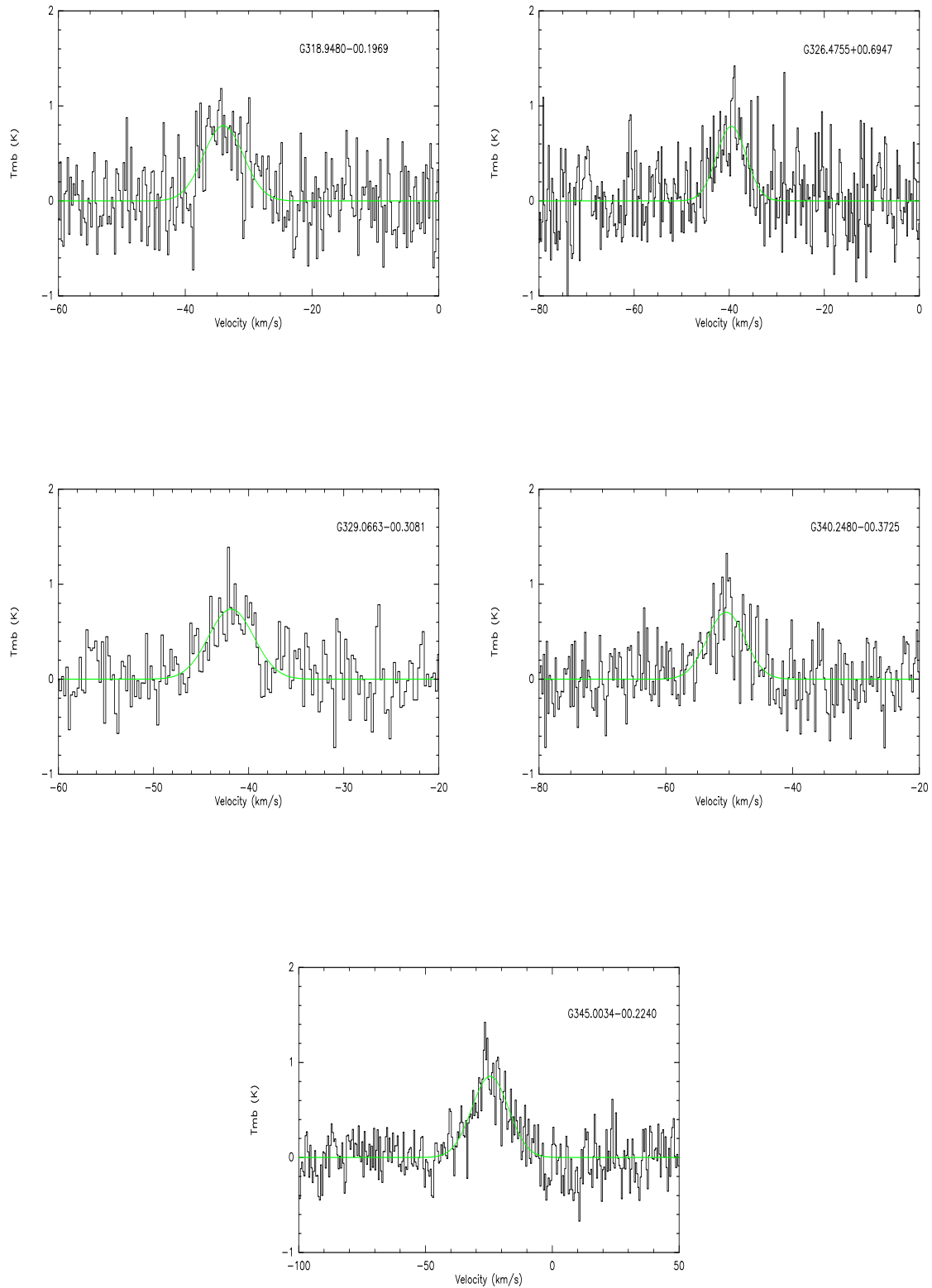


**Figure 5.** SiO (2-1) spectra for five sources in which SiO was detected. The green lines are the Gaussian-fitted lines.



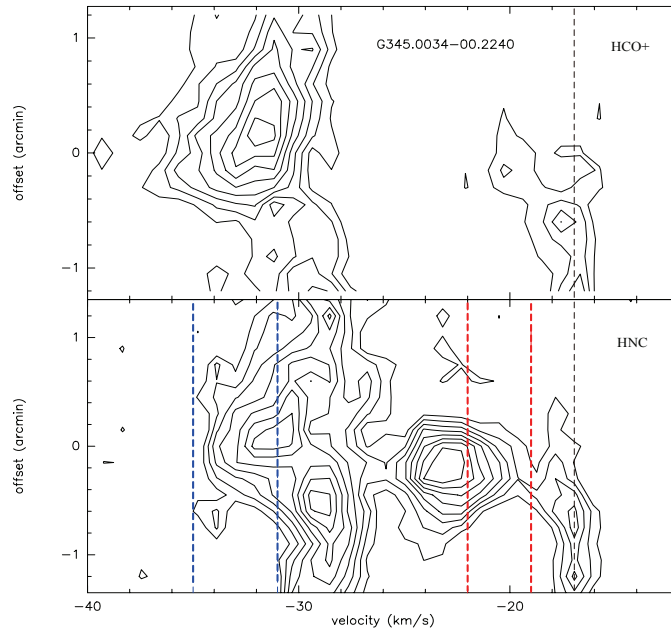


**Figure 6.** PV diagrams made by HCO<sup>+</sup> (top) and HNC (bottom) of G345.0034-00.2240. Contours are 20%, 30%...90% of the peak emissions. The red and blue dashed lines indicate the velocity ranges for the blue and red wings as listed in table 2. The gas at -17 km/s is possibly unrelated to this source.

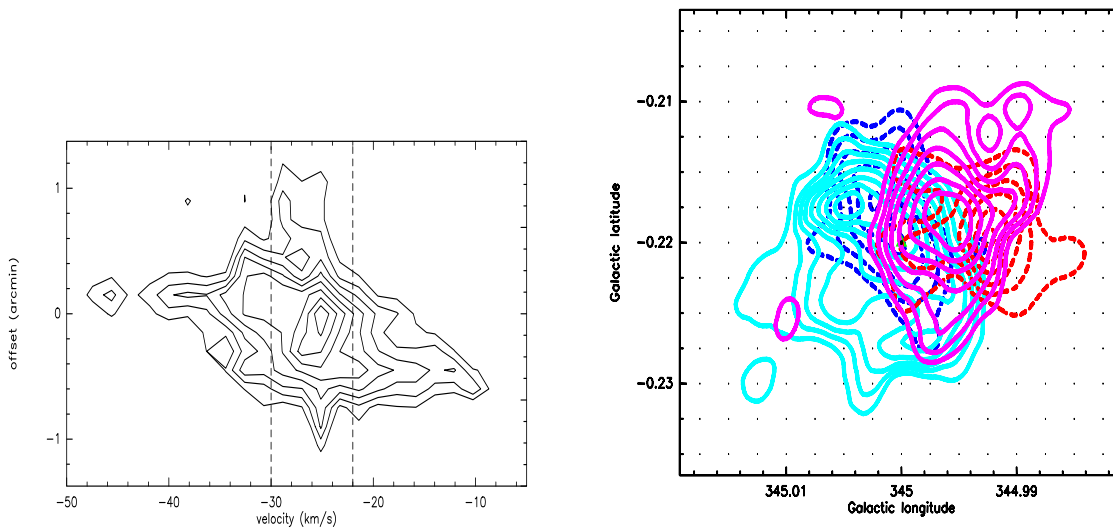


**Figure 7.** Left: SiO PV diagram of G345.0034-00.2240 cut along east-west direction. Contour levels are 30%, 40%...90% of the peak emission. Right: Outflow traced by SiO (dashed red and blue contours) superimposed with HNC<sup>+</sup> wing emissions (cyan and pink contours).

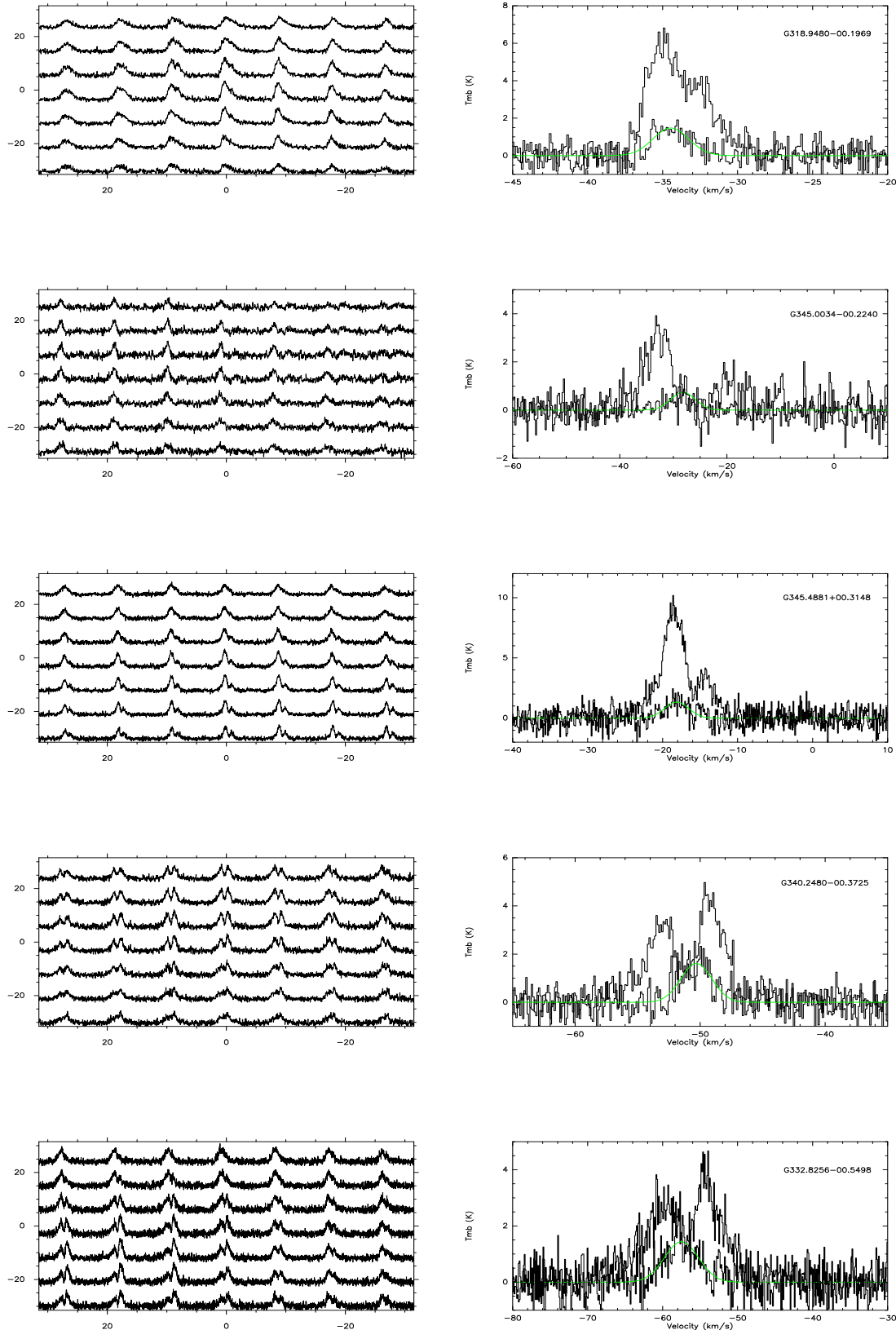


**Figure 8.** From the top and bottom panels present G318.9480-00.1969, G345.0034-00.2240, G345.4881+00.3148, G340.2480-00.3725 and G332.8256-00.5498  $\text{HCO}^+$  mapping observations (left) and its central spectra of  $\text{HCO}^+$  and  $\text{H}^{13}\text{CO}^+$  (right). The green lines are the  $\text{H}^{13}\text{CO}^+$  Gaussian-fitted lines.

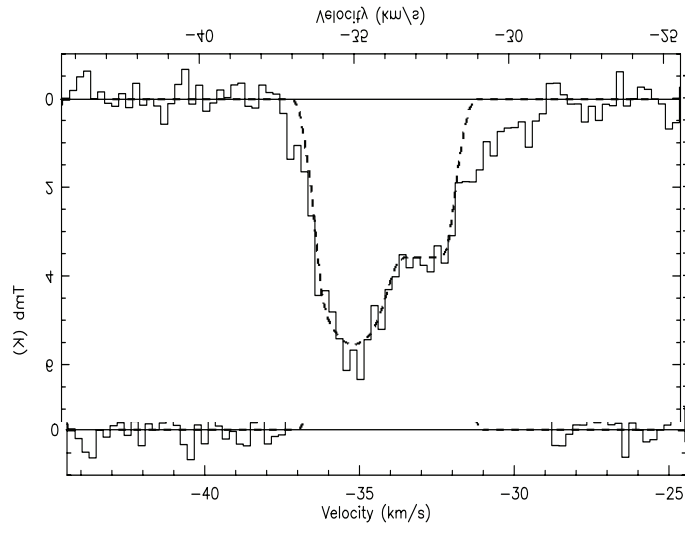


**Figure 9.** A comparison of the observed (solid) and model (dashed) HCO<sup>+</sup> spectra of G318.9480-00.1969.

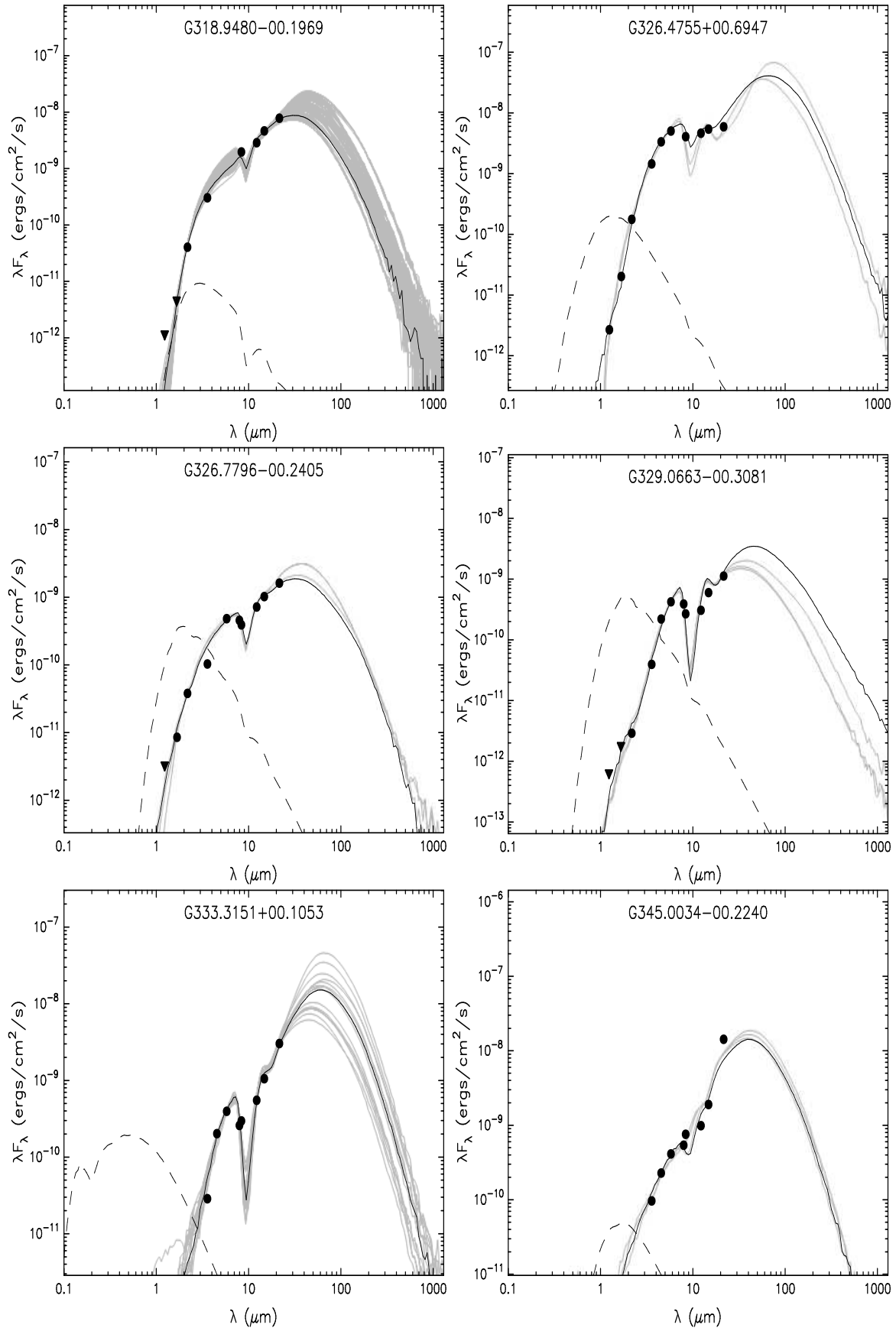


**Figure 10.** The SED fitting models. The dashed line represents the stellar photosphere model. The black line represents the best-fitting SED, and the gray lines represent all the other acceptable YSO fits.

# Molecular line study of massive star forming regions from the RMS survey

Naiping Yu<sup>1,2,3\*</sup> and Jun-Jie Wang<sup>1,2\*†</sup>

<sup>1</sup>National Astronomical Observatories, Chinese Academy of Sciences, Beijing 100012, China

<sup>2</sup>NAOC-TU Joint Center for Astrophysics, Lhasa 850000, China

<sup>3</sup>Graduate School of the Chinese Academy of Sciences, Beijing 100080, China

Accepted 20\*\* December 15. Received 20\*\* December 14

## ABSTRACT

In this paper we selected a sample of massive star forming regions from the Red MSX Source (RMS) survey, to study star formation activities, mainly outflow and inflow signatures. We used the following transitions in our analysis:  $\text{HCO}^+(1-0)$ ,  $\text{H}^{13}\text{CO}^+(1-0)$  and  $\text{SiO}(2-1)$  from the Millimeter Astronomy Legacy Team Survey at 90 GHz (MALT90). Nine sources in our sample are radio-quiet while the other eleven have radio emissions. Twelve sources have outflow activities while only three show inflow signatures in all. We suggest the low ratio inflow detected was mainly caused by beam dilution of the telescope. All the three inflow candidates have outflow. We also found the direction of outflow in G345.0034-00.2240 was different by  $\text{HCO}^+(1-0)$  and  $\text{SiO}(2-1)$  analysis. A simple model of G318.9480-00.1969 shows it has an infall velocity of about  $1.8 \text{ km s}^{-1}$ . The spectral energy distribution (SED) shows our sources are probably massive and intermediate-massive star formation regions.

**Key words:** ISM: molecular - ISM: outflows and inflow - ISM: structure - stars: formation - stars: protostars

## 1 INTRODUCTION

Massive stars have a deep impact on the evolution of galaxies. During their short lives, they determine the main chemical and physical properties of the nearby interstellar medium (ISM). Both theory and observations demonstrate they could hamper or trigger the next generation of star formation, by the expansion of HII regions and supernova explosions at the end of their lives (e.g. Elmegreen & Lada 1977; Lefloch & Lazareff 1994;). However, their formation mechanism is still poorly understood as they used to form in clusters, and detail study of massive star formation is further hampered by their short lives, far distance, rare sources and extensive dust extinctions. Several models have been proposed that high-mass stars could form by accretion driven formation through massive disks (e.g. Keto et al. 2002), competitive accretion in dense clusters (Bonnell et al. 2004), ionized accretion (Keto & Wood, 2006), and mergers of several low-mass stars (Bonnell et al. 1998). The former three models are similar to that of low-mass star formation, accompanied by outflow during the process of gravitational collapse. Recent observations appear to favor the former three mechanism as stellar mergers require a high stellar density. Given the accretion timescales in massive star-forming regions are much shorter than in low mass star-forming regions, the nuclear burning of hydrogen inside take place while massive stars are still accreting, which

means there is no pre-main-sequence stage for massive star formation. Then substantial UV photons and ionized stellar winds rapidly ionize the surrounding hydrogen, forming a hyper-compact HII region (HCHII) or ultracompact HII region (UCHII). Many questions are still unclear whether accretion could be halted by the strong outward radiation and thermal pressure. Does it continue in an ionized form? Does it continue through a molecular or ionized disk?

In recent years several attempts have been taken to search for massive young stellar objects (MYSOs), using color selection criteria and the IRAS point source catalogue (e.g. Molinari et al. 1996; Sridharan et al. 2002). However, these samples tend to be biased towards bright, isolated sources and avoid dense clustered environments and the Galactic mid-plane, as the large IRAS beam ( $\sim 3\text{-}5'$  at  $100 \mu\text{m}$ ). By comparing the the colors of sources from the MSX and 2MASS point source to those known MYSOs, Lumsden et al. (2002) identified approximately 2000 MYSO candidates. The Red MSX Source (RMS) survey is an ongoing multi-wavelength observational programme to provide us the largest MYSO sample for statistical studies by now. Using the Australia Telescope Compact Array (ATCA), Urquhart et al. (2007a) completed the 5 GHz observations of the 892 RMS sources in the southern sky. This programme divided these sources mainly into two groups: HII regions (UCHII and HCHII) and real MYSOs candidates. To obtain kinematic distances, Urquhart et al. (2007b; 2008) made  $^{13}\text{CO}$  (1-0) and (2-1) observations at Mopra, Onsala and Purple Mountain Observatory (PMO) 13.7 m telescope, and the 15 m James Clerk Maxwell Telescope (JCMT), as well as archival data extracted from the Galactic

\* E-mail: yunaiping09@mails.gucas.ac.cn

†

**Table 1.** List of our sources

MSX name	RA (J2000)	Dec. (J2000)	D (kpc)	SUMSS	Log (Lum) ( $L_{\odot}$ )
G314.2204+00.2726	14:25:13.03	-60:31:38.9	...	N <sup>a</sup>	...
G327.3017-00.5382	15:53:00.76	-54:34:53.0	2.9	Y <sup>b</sup>	3.7
G328.5759-00.5285	15:59:38.44	-53:45:18.3	3.6	Y	...
G330.8708-00.3715	16:10:19.00	-52:06:38.5	4.1	Y	3.9
G327.4014+00.4454	15:49:19.37	-53:45:14.5	5.2/9.1	N	...
G329.3371+00.1469	16:00:33.13	-52:44:47.1	7.0	Y	6.1
G332.8256-00.5498	16:20:11.18	-50:53:17.5	3.96	Y	5.4
G333.0162+00.7615	16:15:18.64	-49:48:55.0	3.3	Y	<4.8
G340.2480-00.3725	16:49:30.14	-45:17:48.4	3.9	N	4.5
G340.2768-00.2104	16:48:54.11	-45:10:14.1	...	N	...
G344.4257+00.0451	17:02:09.65	-41:46:46.2	5.0	N	4.9
G345.4881+00.3148	17:04:28.17	-40:46:22.4	2.1	N	4.9

a: N denotes sources not in the SUMSS survey area except G314.2204+00.2726 and G327.4014+00.4454 which are not detected.

b: Y denotes sources detected by SUMSS.

Ring Survey (GRS). They found approximately 56% of all detections have resulted in at least two components. In order to identify a more reliable molecular component, further observations like water and methanol masers, less abundant but denser gas molecular traces like CS (2-1) have to be taken. Based on these observations, we selected twenty RMS sources to study star formation activities (mainly outflow and inflow signatures). Our source selection criteria include: (1) sources should not be on the edge of known HII or supernova regions, considered the large beam ( $\sim 38''$ ) of the 22 m Mopra telescope; (2) According to the observations of ATCA (Urquhart et al. 2007a), sources should be radio quiet or have a simple spherical/unresolved morphology; (3) All sources should be detected by the Millimeter Astronomy Legacy Team Survey at 90 GHz (MALT90) and do not have multiple molecular components. The formations of the selected twenty sources are listed in table 1.

## 2 DATE

The Millimeter Astronomy Legacy Team 90 GHz survey is a large international project aimed at characterizing the sites within our Galaxy where high-mass stars will form. The survey covers a Galactic latitude range of  $\sim -60$  to  $\sim 15^{\circ}$  and Galactic longitude range of  $-1$  to  $+1^{\circ}$ . The observations were carried out with the newly upgraded Mopra Spectrometer (MOPS). The full 8 GHz bandwidth of MOPS was split into 16 zoom bands of 138 MHz each providing a velocity resolution of  $\sim 0.11$  km s<sup>-1</sup> in each band. The angular resolution of Mopra is about 38 arcsec, with beam efficiency between 0.49 at 86 GHz and 0.42 at 115 GHz (Ladd et al. 2005). The maps were made with  $9''$  spacing between adjacent rows. More information about this survey can be found in Foster et al. (2011). The data processing was conducted using Gildas and line parameters (peak intensity, central velocity, FWHM) are obtained by Gaussian fitting.

## 3 RESULTS

Infall and outflow are two of the most important elements to understand the theories of massive star formation. Infall can act to replenish disk material as mass accretes onto a protostar, while outflows serve as a release mechanism for the angular momentum

that builds up during the accretion process. These motions can be studied by investigating the profiles of optically thick and optically thin molecular lines. Blue asymmetric structure, named “blue profile”, a combination of a double peak with a brighter blue peak or a skewed single blue peak in optically thick lines (Mardones et al. 1997) suggests the presence of infalling gas (Sun et al. 2008), which is consistent with the presence of a YSO accreting material. Surely blue profile may also be caused by rotation and outflow. However, infall motion is the only process that would produce consistently the blue profile. Outflow and rotation only produce a blue asymmetric line profile along a particular line of sight to a source (Sun et al. 2008). Besides, SiO is also a well-known tracer of recent outflow. In the cold diffuse ISM, the element of Si is regarded to frozen into dust grains, unless shocks caused by outflow and/or the expansion of HII regions pass through and sublime Si into gas phase. Thus, the detections of SiO emissions from MYSOs could always be equal to the detections of recent outflow activities in these regions. In the following sections, we use position-velocity (PV) diagram of HCO<sup>+</sup> (1-0) and SiO (2-1) detect outflows in our sample. Three sources in our sample also show blue profile. For G318.9480-00.1969, we also employed the three dimensional radiative-transfer code RADMC3D developed by C. Dullemond<sup>1</sup> to compute the HCO<sup>+</sup> (1-0) line emission of an infalling model.

### 3.1 Outflow signatures detected by HCO<sup>+</sup> (1-0) and SiO (2-0)

Outflow makes an important contribution to the line wing emission of HCO<sup>+</sup> (1-0), as it becomes optically thick quickly in dense gas regions. Five HCO<sup>+</sup> (1-0) PV diagrams of our nine MYSOs sources and five in eleven HII regions show distinct wing emissions (figure 1 and figure 2, respectively). Figure 3 and figure 4 show the integrated maps by integrating wing emissions of our MYSOs and HII regions, respectively. All the detected outflows of MYSOs in our sample are unresolved, and most red and blue lobes of HII regions have different directions with the RMS sources located at the center. Considering the mean distance of our RMS sources with radio emission ( $\sim 5.7$  kpc) is larger than those radio quiet ( $\sim 2.6$  kpc), our result agrees the MYSO candidates should be in much early

<sup>1</sup> See <http://www.ita.uni-heidelberg.de/dullemond/software/radmc-3d/>

**Table 2.** Outflow parameters

Outflow sources	$\Delta b$ (km s <sup>-1</sup> )	$\Delta r$ (km s <sup>-1</sup> )	M (M <sub>⊙</sub> )	P (M <sub>⊙</sub> km s <sup>-1</sup> )	E (M <sub>⊙</sub> [km s <sup>-1</sup> ] <sup>2</sup> )
G314.2204+00.2726	(-68,-62)	(-59,-54)	...	...	...
G328.5759-00.5285	(-54,-49)	(-45.5,-40)	879	6153	21536
G327.4014+00.4454 <sup>a</sup>	(-86,-82)	(-71,-75)	40	292	1086
G329.3371+00.1469	(-114,-109.5)	(-106,-100)	241	1750	6466
G332.8256-00.5498	(-66,-61)	(-54,-48)	90	805	3625
G333.0162+00.7615	(-55,-51)	(-46,-43)	95	566	1721
G340.2480-00.3725	(-57,-53)	(-49,-46)	94	502	1387
G345.4881+00.3148	(-24,-20)	(-14,-10)	20	139	490

stage of HCHII/UCHII regions. We should mention the outflow detection rate is just a low limit because of beam dilution, especially for the MSYO candidates. Figure 5 shows the detected SiO spectra toward peak emission. Models and observations also suggest SiO may be due to the photodissociated region (PDR) surrounding the UCHII region and not an outflow (e.g. Schilke et al. 2001; Shepherd et al. 2004). For the MSYO candidates, as they are radio quiet, SiO emissions triggered by PDR are impossible, so they must be due to outflow activities. Outflow activity was not found in G318.9480-00.1969. However, it shows SiO emissions. Outflow(s) in this source may be heavily diluted. The SiO spectra of UCHII region G345.0034-00.2240 extends from -8 km s<sup>-1</sup> to -48 km s<sup>-1</sup>, suggesting outflow activities. PV diagram for SiO in G345.0034-00.2240 cut along east-west direction is shown in figure 6. Figure 7 shows the maps of the integrated blue and red shifted SiO (2-1) emission (the dash contours). It can be noted SiO traces the inner region of the outflow, compared to HCO<sup>+</sup>. More interestingly, the outflow direction traced by SiO is a little different from that traced by HCO<sup>+</sup>. Is it caused by multiple outflows with different ages, or just single outflow changes its direction in large area? Deeper observations should be carried out to answer this question.

Assuming that HCO<sup>+</sup> (1-0) emission in the line wings to be optically thin and Local Thermodynamic Equilibrium (LTE),  $X(\text{HCO}) = [\text{HCO}]/[\text{H}_2] = 10^{-8}$  (Turner et al. 1997) and  $T_{ex} = 15$  K, we derive the column density from:

$$N(\text{HCO}) = Q(T_{ex}) \frac{8\pi\nu_0^3 g_l}{c^3 g_u A_{ul}} \frac{1}{g_l} [1 - e^{-h\nu_0/kT_{ex}}]^{-1} \int \tau dv \quad (1)$$

where  $\nu_0$ ,  $g_u$ ,  $g_l$  and  $A_{ul}$  are the rest frequency, the upper and lower level degeneracies and the Einstein's coefficient of HCO,  $Q(T_{ex})$  is the partition function, and  $c$  is the speed of light. On the other hand, by assuming HCO emission is optically thin in the line wings, we use the approximation:

$$\int \tau dv = \frac{1}{J(T_{ex}) - J(T_{bg})} \int T_{mb} dv \quad (2)$$

The derived parameters are shown in table 2.

### 3.2 Infall signatures detected by HCO<sup>+</sup> (1-0) and H<sup>13</sup>CO<sup>+</sup> (1-0)

The HCO<sup>+</sup> (1-0) spectra of four sources (figure 8) do not have a simple Gaussian shape, presenting spectral wings and absorption dips where is the emission peak of H<sup>13</sup>CO<sup>+</sup> (1-0), which suggest that the molecular gas are affected by the dynamics of these star-forming regions. Mapping observations could help us to distinguish whether this was caused by inward motions or other dynamics such as outflow, rotation and expansions of HII regions. Figure 8

(the left panels) show the mapping observations towards our four sources with double peaked HCO<sup>+</sup> (1-0) emissions. Three sources except G340.248-00.376 show consistent blue profile, indicating infall motions. Outflow activities are also detected in these regions (see section 3.1). Like low star formation mechanical, massive stars in these regions are also forming through accretion-outflow process. For G345.0034-00.2240, the detection of recent outflow activity traced by SiO and the appearance to be undergoing infall in this region suggest ongoing accretion beyond the onset of the HII region. The outward radiation and thermal pressure from the central massive star(s) do not seem to strong enough to halt accretion. Like G10.6-0.4 (Keto & Wood 2006), accretion flow in this region may be ionized.

Klaassen et al. (2007,2012) obtained JCMT observations of HCO<sup>+</sup>/H<sup>13</sup>CO<sup>+</sup> (4-3) to trace large scale inward motions in a sample of massive star-forming regions (mainly MYSOs, HCHII and UCHII regions) The infall rate in our sample is relatively low compared their work. This may be partly due to their higher resolution (15'' vs. 38''). Besides, the higher J = 4-3 transition does not self absorb as readily as J = 1-0, making it a better asymmetry tracer. Only one source in our MYSO candidates show infall signature. This is because the infall area with MYSO is relatively smaller than that in UCHII regions, and then more likely to be beam diluted.

### 3.3 A simple model of G318.9480-00.1969

G318.9480-00.1969 is the only MYSO candidate detected infall signatures. In this section, we try to constrain the spatial and dynamic structure of G318.9480-00.1969, using a radiative-transfer model that reproduce HCO<sup>+</sup> (1-0) line. We employed the three dimensional radiative-transfer code RADMC-3D (developed by C.Dullemond) to compute the dust temperature heated by a central stellar and line emission of an infall model. The dust opacity is from Ossenkopf & Henning (1994) without grain mantles or coagulation. The molecular data of HCO<sup>+</sup> comes from the Leiden LAMDA database<sup>2</sup>. The line transfer assumes the gas temperature to be equal to the dust temperature and LTE (full non-LTE radiation transfer is also planned for RADMC-3D).

In our model, the volume density follows a radial power law,  $n \propto r^{-1.5}$ , with a total mass of 31 M<sub>⊙</sub> (estimated from our observations) within a box of (4000 AU)<sup>3</sup>. At the center lies a star of 10 M<sub>⊙</sub> (see section 3.4). The gas has a turbulence velocity of 0.5 km s<sup>-1</sup> and is radially infalling with 1.8 km s<sup>-1</sup> to the central star. A comparison of the observed and model spectra is shown in figure

<sup>2</sup> <http://www.strw.leidenuniv.nl/~moldata>

9. At the center spectra our model matches well this the observation. However, the observed line seems to have line wing emissions, probably caused by outflow activities. The detected SiO spectra indeed imply beam diluted outflow(s) in this region. Even though our model is consistent with the data, we should realize it does not provide errors of the parameters, and different models may also fit as well.

### 3.4 Spectral energy distribution

In this section, we try to fit the spectral energy distribution (SED) of our sources using the tool developed by Robitaille et al. (2007). Briefly, the SED-fitting tool works as a regression method to find the SEDs within a specified  $\chi^2$  from a large grid of models after fitting the input data points. The grid of models contains stellar masses, disk masses, mass accretion rates, and line-of-sight (LOS) inclinations. The grid of YSO models was computed by Robitaille et al. (2006) using the 20,000 two-dimensional radiation transfer models from Whitney et al. (2003a, 2003b, 2004). Each YSO model has SEDs for 10 viewing angles (inclinations), so the total YSO grid consists of 200,000 SEDs. We use the archival data from 2MASS, IRAC of Spitzer, MSX to fits the SED of our sources. In addition to the best-fit model (the black line in figure 10), we also show the range of possible parameters that can be derived from models within the range of  $\chi^2/\nu - \chi^2_{best}/\nu \leq 4$  ( $\nu$  represents the number of data points). The derived model parameters are listed in table 4 and the resulting SEDs are shown in figure 10. The SED shows our sources are probably massive and intermediate-massive star formation regions, with masses ranging from 5 - 10  $M_{\odot}$ .

## 4 CONCLUSION

In this paper we selected a sample of massive star forming regions from the Red MSX Source (RMS) survey, to study star formation activities, mainly outflow and inflow signatures. We used the following transitions in our analysis:  $\text{HCO}^+(1-0)$ ,  $\text{H}^{13}\text{CO}^+(1-0)$  and  $\text{SiO}(2-1)$  from the Millimeter Astronomy Legacy Team Survey at 90 GHz (MALT90). Nine sources in our sample are radio-quiet while the other eleven have radio emissions. Twelve sources have outflow activities while only three show inflow signatures in all. We suggest the low ratio inflow detected was mainly caused by beam dilution of the telescope. All the three inflow candidates have outflow. We also found the direction of outflow in G345.0034-00.2240 was different by  $\text{HCO}^+(1-0)$  and  $\text{SiO}(2-1)$  analysis. A simple model of G318.9480-00.1969 shows it has an infall velocity of about 1.8  $\text{km s}^{-1}$ . The spectral energy distribution (SED) shows our sources are probably massive and intermediate-massive star formation regions.



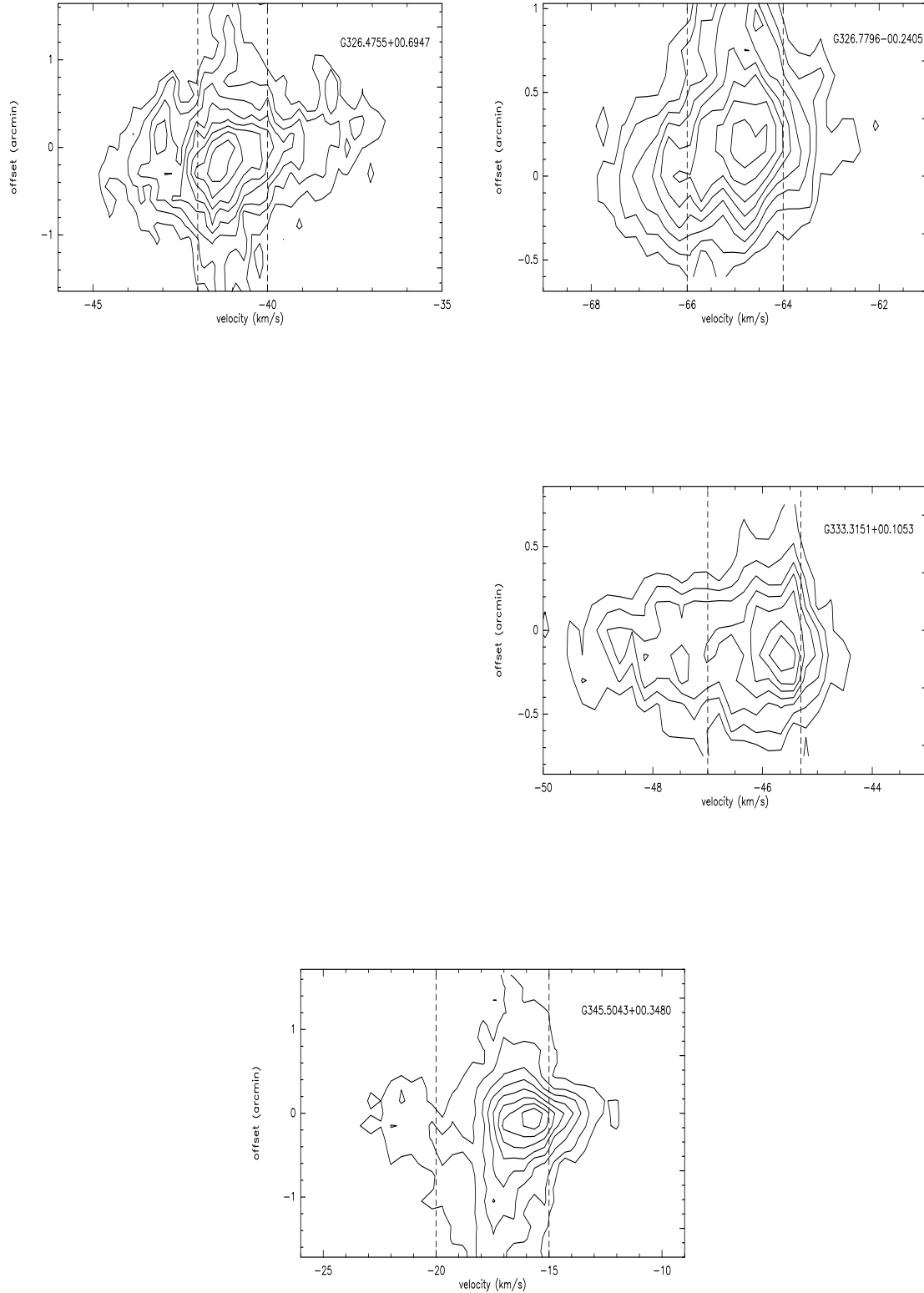


**Figure 1.** Two examples of the SED fitting model. The dashed line represents the stellar photosphere model. The black line represents the best-fitting SED, and the gray lines represent all the other acceptable YSO fits.

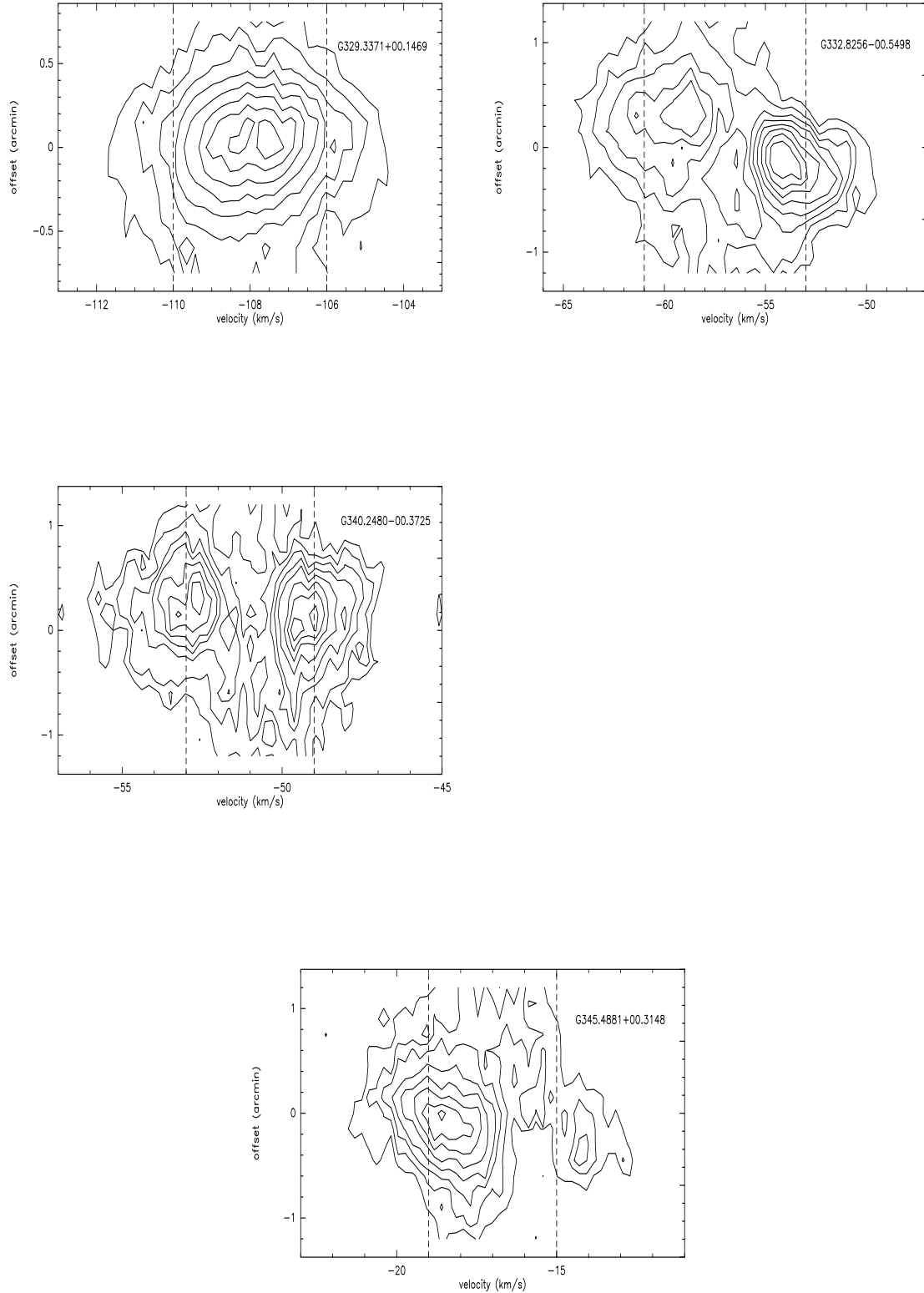


**Figure 2.** Two examples of the SED fitting model. The dashed line represents the stellar photosphere model. The black line represents the best-fitting SED, and the gray lines represent all the other acceptable YSO fits.

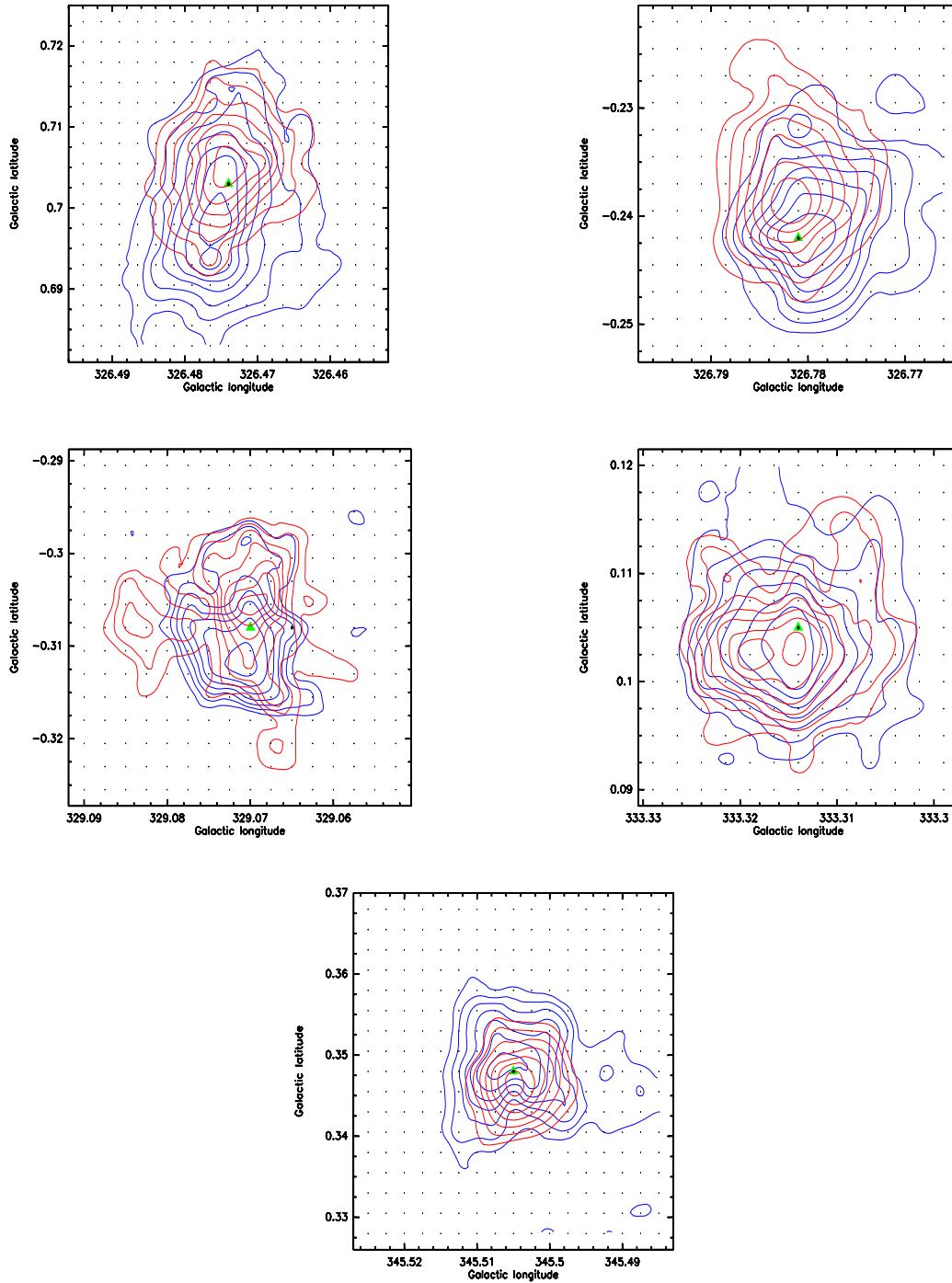


**Figure 3.** Two examples of the SED fitting model. The dashed line represents the stellar photosphere model. The black line represents the best-fitting SED, and the gray lines represent all the other acceptable YSO fits.

**REFERENCES**

Bonnell, I.A. et al 1998, MNRAS, 298, 93  
 Bonnell, I.A. et al. 2004, MNRAS, 349, 735  
 Elmegreen, B. G., Lada C.J., 1977, ApJ, 214, 725  
 Foster J.B., et al. 2011, ApJS, 197, 25  
 Keto, E. 2002, ApJ, 580, 980  
 Keto, E., Wood, K. 2006, ApJ, 637, 850

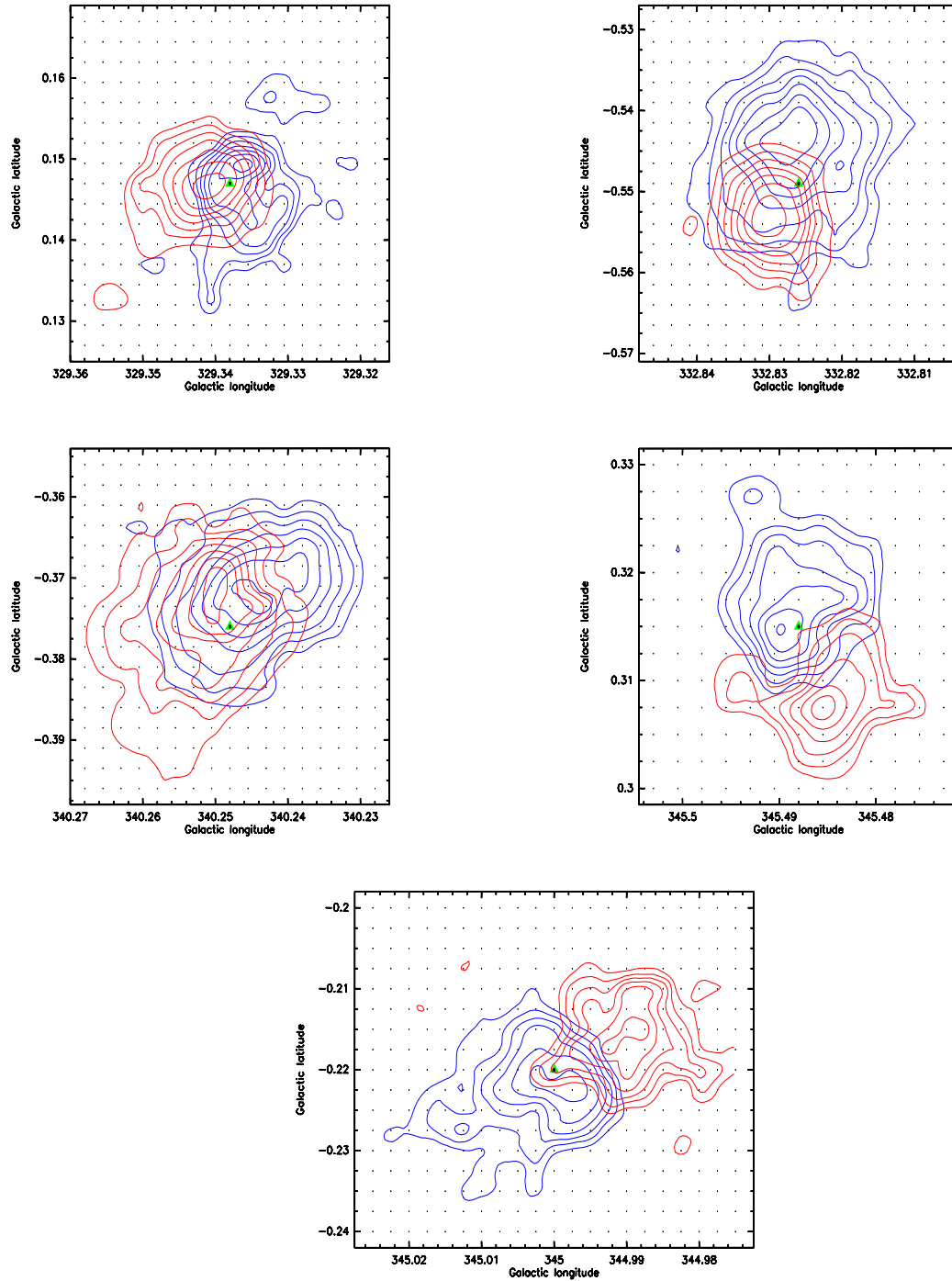


**Figure 4.** Two examples of the SED fitting model. The dashed line represents the stellar photosphere model. The black line represents the best-fitting SED, and the gray lines represent all the other acceptable YSO fits.

Klaassen P.D., Wilson C.D., 2007, *ApJ*, 663, 1092  
 Klaassen P.D., Testi, L., Beuther, H., 2012, *A&A*, 538, 140  
 Ladd N., Purcell, C., Wong, T., & Robertson, S. 2005, *PASA*, 22, 62  
 Lefloch, B., Lazareff, B., 1994, *A&A*, 289, 559  
 Lumsden, S. L., Hoare, M. G., Oudmaijer, R. D., Richards, D. 2002, *MNRAS*, 336, 621  
 Mardones, D., Myers, P. C., Tafalla, M. et al. 1997, *ApJ*, 489, 719  
 Molinari, S., Brand, J., Cesaroni, R., Palla, F. 1996, *A&A*, 308, 573

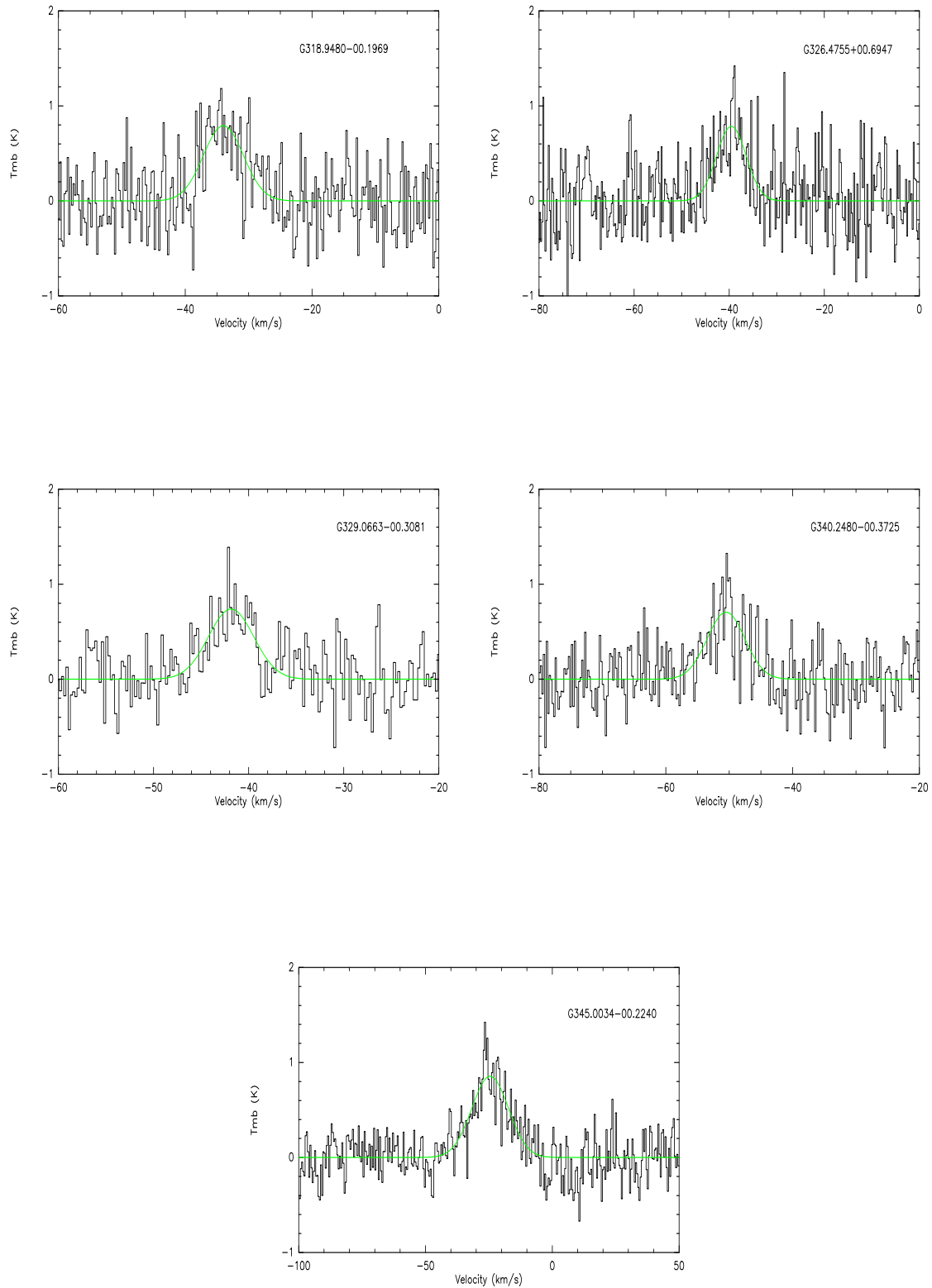


**Figure 5.** Two examples of the SED fitting model. The dashed line represents the stellar photosphere model. The black line represents the best-fitting SED, and the gray lines represent all the other acceptable YSO fits.

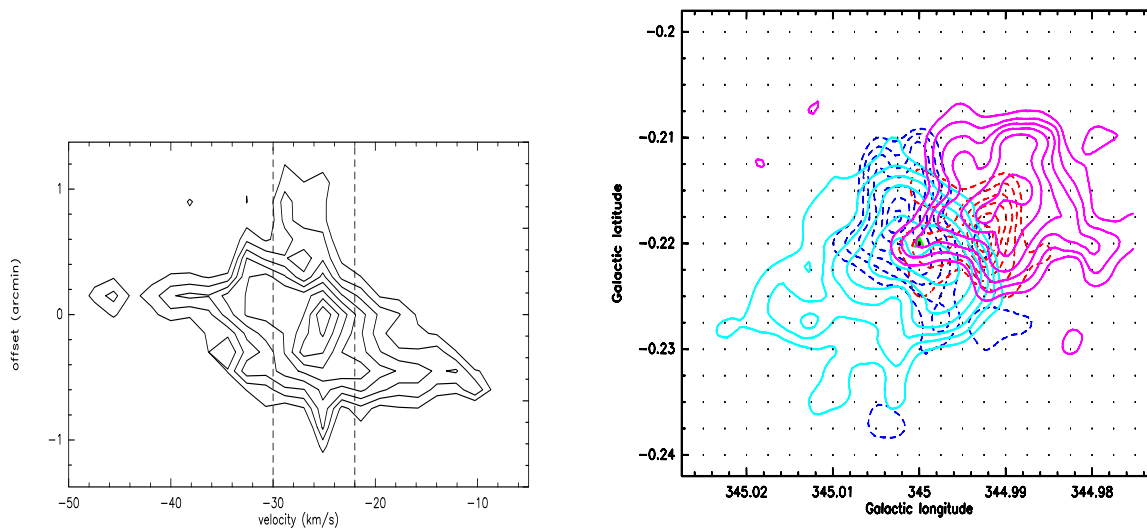


**Figure 6.** Two examples of the SED fitting model. The dashed line represents the stellar photosphere model. The black line represents the best-fitting SED, and the gray lines represent all the other acceptable YSO fits.

- Ossenkopf, V., & Henning, T. 1994, *A&A*, 291, 943  
 Robitaille, T. P., Whitney, B. A., Indebetouw, R., Wood, K., Denzmore, P., 2006, *ApJS*, 167, 256  
 Robitaille, T. P., Whitney, B. A., Indebetouw, R., Wood, K., 2007, *ApJS*, 169, 328  
 Schilke, P., Pineau des Forêts, G., Walmsley, C.M., et al., 2001, *A&A*, 372, 291  
 Shepherd, D.S., Kurtz, S.E., Testi, L. 2004, *ApJ*, 601, 952  
 Sridharan, T. K., Schilke, P., Menten, K. M., Wyrowski, F. 2002, *ApJ*, 566, 931  
 Sun Yan, Gao Yu, 2009, *MNRAS*, 392, 170  
 Urquhart, J. S., Busfield, A. L., Hoare, M. G., et al. 2007a, *A&A*, 461, 11  
 Urquhart, J. S., et al. 2007b, *A&A*, 474, 891  
 Urquhart, J. S., et al. 2008, *A&A*, 487, 253  
 Whitney, B. A., Indebetouw, R., Bjorkman, J.E., Wood, K., 2004, *ApJ*, 617, 1177  
 Whitney, B. A., Wood, K., Bjorkman, J. E., Cohen, M., 2003a, *ApJ*, 598, 1079  
 Whitney, B. A., Wood, K., Bjorkman, J. E., Wolff, M. J., 2003b, *ApJ*, 591, 1049

This paper has been typeset from a  $\text{\TeX}/\text{\LaTeX}$  file prepared by the author.

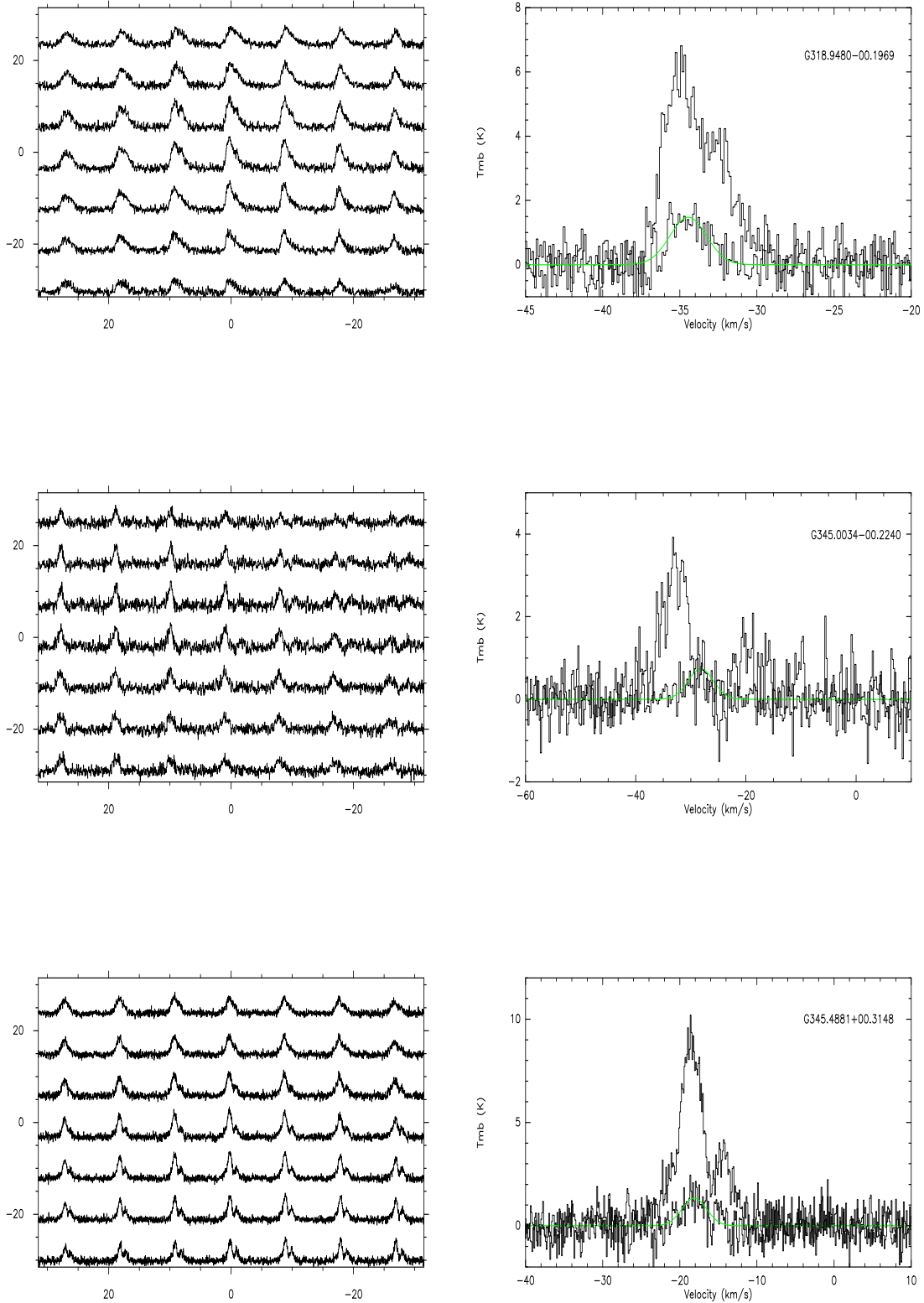


**Figure 7.** Two examples of the SED fitting model. The dashed line represents the stellar photosphere model. The black line represents the best-fitting SED, and the gray lines represent all the other acceptable YSO fits.

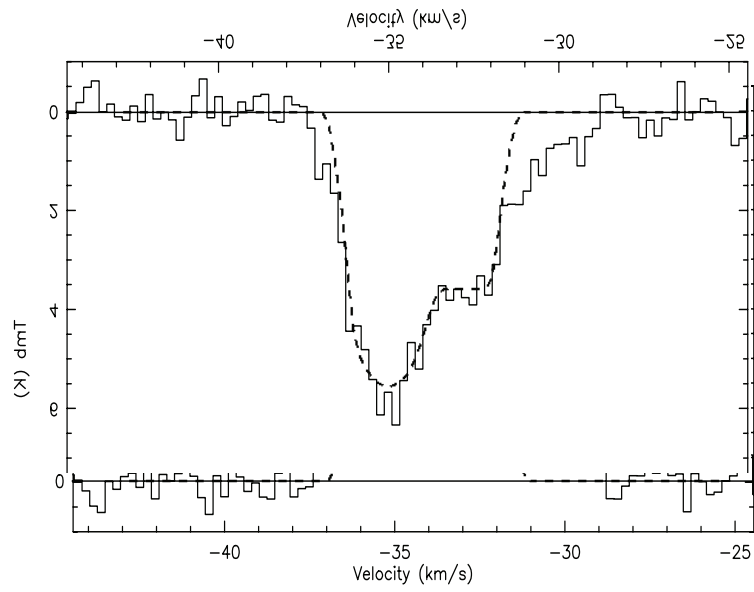


**Figure 8.** Two examples of the SED fitting model. The dashed line represents the stellar photosphere model. The black line represents the best-fitting SED, and the gray lines represent all the other acceptable YSO fits.



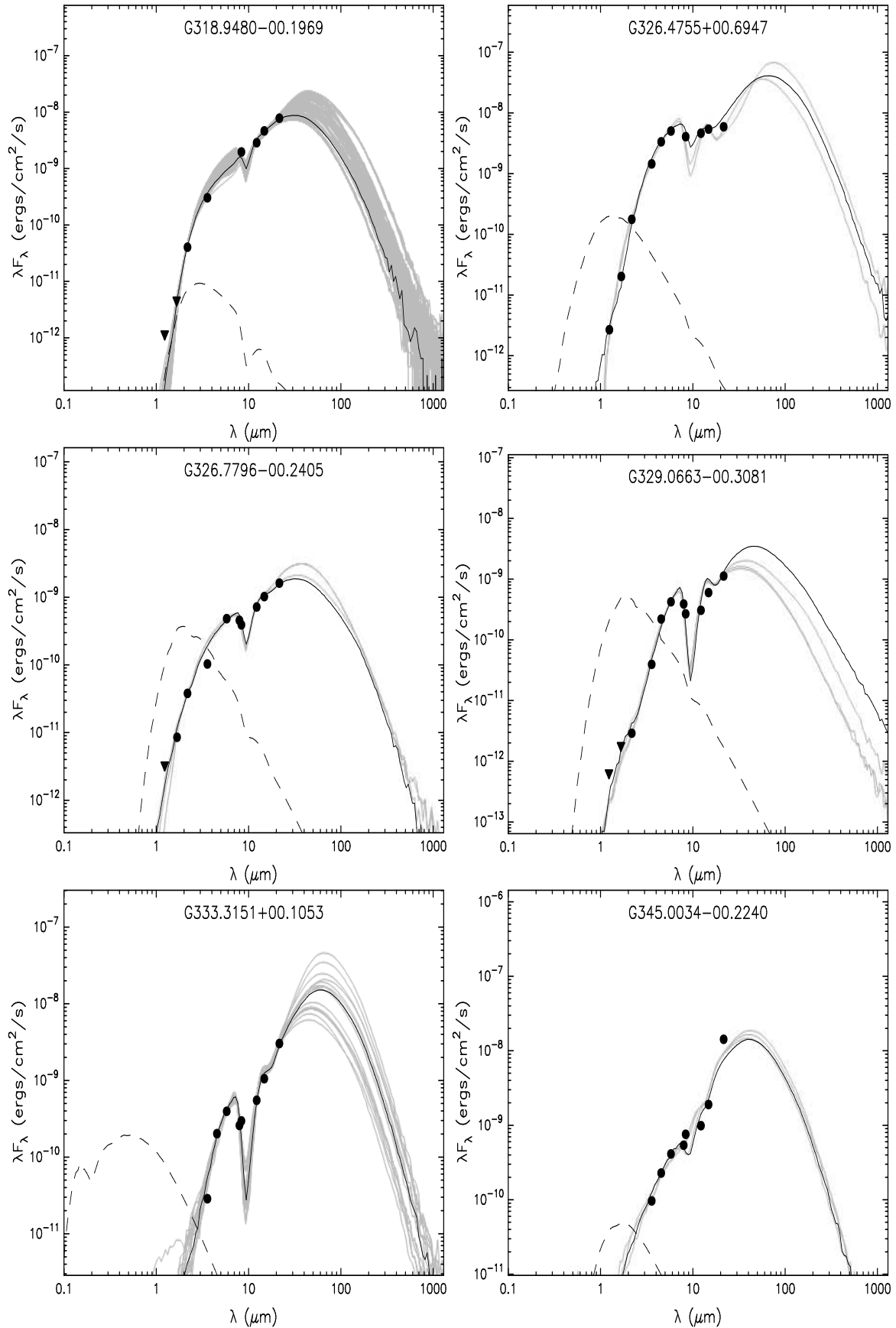


**Figure 9.** Two examples of the SED fitting model. The dashed line represents the stellar photosphere model. The black line represents the best-fitting SED, and the gray lines represent all the other acceptable YSO fits.

# Molecular line study of massive star forming regions from the RMS survey

Naiping Yu<sup>1,2,3\*</sup> and Jun-Jie Wang<sup>1,2\*†</sup>

<sup>1</sup>*National Astronomical Observatories, Chinese Academy of Sciences, Beijing 100012, China*

<sup>2</sup>*NAOC-TU Joint Center for Astrophysics, Lhasa 850000, China*

<sup>3</sup>*Graduate School of the Chinese Academy of Sciences, Beijing 100080, China*

Accepted 20\*\* December 15. Received 20\*\* December 14

## ABSTRACT

In this paper we selected a sample of massive star forming regions from the Red MSX Source (RMS) survey, to study star formation activities, mainly outflow and inflow signatures. We used the following transitions in our analysis: HCO<sup>+</sup>(1-0), H<sup>13</sup>CO<sup>+</sup>(1-0) and SiO(2-1) from the Millimeter Astronomy Legacy Team Survey at 90 GHz (MALT90). Nine sources in our sample are radio-quiet while the other eleven have radio emissions. Twelve sources have outflow activities while only three show inflow signatures in all. We suggest the low ratio inflow detected was mainly caused by beam dilution of the telescope. All the three inflow candidates have outflow. We also found the direction of outflow in G345.0034-00.2240 was different by HCO<sup>+</sup>(1-0) and SiO(2-1) analysis. A simple model of G318.9480-00.1969 shows it has an infall velocity of about 1.8 km s<sup>-1</sup>. The spectral energy distribution (SED) shows our sources are probably massive and intermediate-massive star formation regions.

**Key words:** ISM: molecular - ISM: outflows and inflow - ISM: structure - stars: formation - stars: protostars

## 1 INTRODUCTION

Massive stars have a deep impact on the evolution of galaxies. During their short lives, they determine the main chemical and physical properties of the nearby interstellar medium (ISM). Both theory and observations demonstrate they could hamper or trigger the next generation of star formation, by the expansion of HII regions and supernova explosions at the end of their lives (e.g. Elmegreen & Lada 1977; Lefloch & Lazareff 1994;). However, their formation mechanism is still poorly understood as they used to form in clusters, and detail study of massive star formation is further hampered by their short lives, far distance, rare sources and extensive dust extinctions. Several models have been proposed that high-mass stars could form by accretion driven formation through massive disks (e.g. Keto et al. 2002), competitive accretion in dense clusters (Bonnell et al. 2004), ionized accretion (Keto & Wood, 2006), and mergers of several low-mass stars (Bonnell et al. 1998). The former three models are similar to that of low-mass star formation, accompanied by outflow during the process of gravitational collapse. Recent observations appear to favor the former three mechanism as stellar mergers require a

high stellar density. Given the accretion timescales in massive star-forming regions are much shorter than in low mass star-forming regions, the nuclear burning of hydrogen inside take place while massive stars are still accreting, which means there is no pre-main-sequence stage for massive star formation. Then substantial UV photons and ionized stellar winds rapidly ionize the surrounding hydrogen, forming a hyper-compact HII region (HCHII) or ultracompact HII region (UCHII). Many questions are still unclear whether accretion could be halted by the strong outward radiation and thermal pressure. Does it continue in an ionized form? Does it continue through a molecular or ionized disk?

In recent years several attempts have been taken to search for massive young stellar objects (MYSOs), using color selection criteria and the IRAS point source catalogue (e.g. Molinari et al. 1996; Sridharan et al. 2002). However, these samples tend to be biased towards bright, isolated sources and avoid dense clustered environments and the Galactic mid-plane, as the large IRAS beam ( $\sim 3\text{-}5'$  at 100  $\mu\text{m}$ ). By comparing the the colors of sources from the MSX and 2MASS point source to those known MYSOs, Lumsden et al. (2002) identified approximately 2000 MYSO candidates. The Red MSX Source (RMS) survey is an ongoing multi-wavelength observational programme to provide us the largest MYSO sample for statistical studies by now. Using the Australia Telescope Compact Array (ATCA),

\* E-mail: yunaiping09@mails.gucas.ac.cn

†

**Table 1.** List of our sources

MSX name	RA (J2000)	Dec. (J2000)	D (kpc)	SUMSS	Log (Lum) ( $L_{\odot}$ )
G314.2204+00.2726	14:25:13.03	-60:31:38.9	...	N <sup>a</sup>	...
G327.3017-00.5382	15:53:00.76	-54:34:53.0	2.9	Y <sup>b</sup>	3.7
G328.5759-00.5285	15:59:38.44	-53:45:18.3	3.6	Y	...
G330.8708-00.3715	16:10:19.00	-52:06:38.5	4.1	Y	3.9
G327.4014+00.4454	15:49:19.37	-53:45:14.5	5.2/9.1	N	...
G329.3371+00.1469	16:00:33.13	-52:44:47.1	7.0	Y	6.1
G332.8256-00.5498	16:20:11.18	-50:53:17.5	3.96	Y	5.4
G333.0162+00.7615	16:15:18.64	-49:48:55.0	3.3	Y	<4.8
G340.2480-00.3725	16:49:30.14	-45:17:48.4	3.9	N	4.5
G340.2768-00.2104	16:48:54.11	-45:10:14.1	...	N	...
G344.4257+00.0451	17:02:09.65	-41:46:46.2	5.0	N	4.9
G345.4881+00.3148	17:04:28.17	-40:46:22.4	2.1	N	4.9

a: N denotes sources not in the SUMSS survey area except G314.2204+00.2726 and G327.4014+00.4454 which are not detected.

b: Y denotes sources detected by SUMSS.

Urquhart et al. (2007a) completed the 5 GHz observations of the 892 RMS sources in the southern sky. This programme divided these sources mainly into two groups: HII regions (UCHII and HCHII) and real MYSOs candidates. To obtain kinematic distances, Urquhart et al. (2007b; 2008) made <sup>13</sup>CO (1-0) and (2-1) observations at Mopra, Onsala and Purple Mountain Observatory (PMO) 13.7 m telescope, and the 15 m James Clerk Maxwell Telescope (JCMT), as well as archival data extracted from the Galactic Ring Survey (GRS). They found approximately 56% of all detections have resulted in at least two components. In order to identify a more reliable molecular component, further observations like water and methanol masers, less abundant but denser gas molecular traces like CS (2-1) have to be taken. Based on these observations, we selected twenty RMS sources to study star formation activities (mainly outflow and inflow signatures). Our source selection criteria include: (1) sources should not be on the edge of known HII or supernova regions, considered the large beam ( $\sim 38''$ ) of the 22 m Mopra telescope; (2) According to the observations of ATCA (Urquhart et al. 2007a), sources should be radio quiet or have a simple spherical/unresolved morphology; (3) All sources should be detected by the Millimeter Astronomy Legacy Team Survey at 90 GHz (MALT90) and do not have multiple molecular components. The formations of the selected twenty sources are listed in table 1.

## 2 DATE

The Millimeter Astronomy Legacy Team 90 GHz survey is a large international project aimed at characterizing the sites within our Galaxy where high-mass stars will form. The survey covers a Galactic latitude range of  $\sim -60$  to  $\sim 15^{\circ}$  and Galactic longitude range of  $-1$  to  $+1^{\circ}$ . The observations were carried out with the newly upgraded Mopra Spectrometer (MOPS). The full 8 GHz bandwidth of MOPS was split into 16 zoom bands of 138 MHz each providing a velocity resolution of  $\sim 0.11$  km s<sup>-1</sup> in each band. The angular resolution of Mopra is about 38 arcsec, with beam efficiency between 0.49 at 86 GHz and 0.42 at 115 GHz (Ladd et al. 2005). The maps were made with  $9''$  spacing between adjacent rows.

More information about this survey can be found in Foster et al. (2011). The data processing was conducted using Gildas and line parameters (peak intensity, central velocity, FWHM) are obtained by Gaussian fitting.

## 3 RESULTS

Infall and outflow are two of the most important elements to understand the theories of massive star formation. Infall can act to replenish disk material as mass accretes onto a protostar, while outflows serve as a release mechanism for the angular momentum that builds up during the accretion process. These motions can be studied by investigating the profiles of optically thick and optically thin molecular lines. Blue asymmetric structure, named “blue profile”, a combination of a double peak with a brighter blue peak or a skewed single blue peak in optically thick lines (Mardones et al. 1997) suggests the presence of infalling gas (Sun et al. 2008), which is consistent with the presence of a YSO accreting material. Surely blue profile may also be caused by rotation and outflow. However, infall motion is the only process that would produce consistently the blue profile. Outflow and rotation only produce a blue asymmetric line profile along a particular line of sight to a source (Sun et al. 2008). Besides, SiO is also a well-known tracer of recent outflow. In the cold diffuse ISM, the element of Si is regarded to frozen into dust grains, unless shocks caused by outflow and/or the expansion of HII regions pass through and sublimate Si into gas phase. Thus, the detections of SiO emissions from MYSOs could always be equal to the detections of recent outflow activities in these regions. In the following sections, we use position-velocity (PV) diagram of HCO<sup>+</sup> (1-0) and SiO (2-1) detect outflows in our sample. Three sources in our sample also show blue profile. For G318.9480-00.1969, we also employed the three dimensional radiative-transfer code RADMC3D developed by C. Dullemond<sup>1</sup> to compute the HCO<sup>+</sup> (1-0) line emission of an infalling model.

<sup>1</sup> See <http://www.ita.uni-heidelberg.de/dullemond/software/radmc-3d/>

**Table 2.** Outflow parameters

Outflow sources	$\Delta b$ (km s <sup>-1</sup> )	$\Delta r$ (km s <sup>-1</sup> )	M (M <sub>⊙</sub> )	P (M <sub>⊙</sub> km s <sup>-1</sup> )	E (M <sub>⊙</sub> [km s <sup>-1</sup> ] <sup>2</sup> )
G314.2204+00.2726	(-68,-62)	(-59,-54)	...	...	...
G328.5759-00.5285	(-54,-49)	(-45.5,-40)	879	6153	21536
G327.4014+00.4454 <sup>a</sup>	(-86,-82)	(-71,-75)	40	292	1086
G329.3371+00.1469	(-114,-109.5)	(-106 -100)	241	1750	6466
G332.8256-00.5498	(-66,-61)	(-54,-48 )	90	805	3625
G333.0162+00.7615	(-55,-51 )	(-46,-43)	95	566	1721
G340.2480-00.3725	(-57,-53)	(-49,-46)	94	502	1387
G345.4881+00.3148	(-24,-20)	(-14,-10)	20	139	490

### 3.1 Outflow signatures detected by HCO<sup>+</sup> (1-0) and SiO (2-0)

Outflow makes an important contribution to the line wing emission of HCO<sup>+</sup> (1-0), as it becomes optically thick quickly in dense gas regions. Five HCO<sup>+</sup> (1-0) PV diagrams of our nine MYSOs sources and five in eleven HII regions show distinct wing emissions (figure 1 and figure 2, respectively). Figure 3 and figure 4 show the integrated maps by integrating wing emissions of our MYSOs and HII regions, respectively. All the detected outflows of MYSOs in our sample are unresolved, and most red and blue lobes of HII regions have different directions with the RMS sources located at the center. Considering the mean distance of our RMS sources with radio emission ( $\sim 5.7$  kpc) is larger than those radio quiet ( $\sim 2.6$  kpc), our result agrees the MYSO candidates should be in much early stage of HCHII/UCHII regions. We should mention the outflow detection rate is just a low limit because of beam dilution, especially for the MYSO candidates. Figure 5 shows the detected SiO spectra toward peak emission. Models and observations also suggest SiO may be due to the photodissociated region (PDR) surrounding the UCHII region and not an outflow (e.g. Schilke et al. 2001; Shepherd et al. 2004). For the MYSO candidates, as they are radio quiet, SiO emissions triggered by PDR are impossible, so they must be due to outflow activities. Outflow activity was not found in G318.9480-00.1969. However, it show SiO emissions. Outflow(s) in this source may be heavily diluted. The SiO spectra of UCHII region G345.0034-00.2240 extends from  $-8$  km s<sup>-1</sup> to  $-48$  km s<sup>-1</sup>, suggesting outflow activities. PV diagram for SiO in G345.0034-00.2240 cut along east-west direction is shown in figure 6. Figure 7 shows the maps of the integrated blue and red shifted SiO (2-1) emission (the dash contours). It can be noted SiO traces the inner region of the outflow, compared to HCO<sup>+</sup>. More interestingly, the outflow direction traced by SiO is a little different from that traced by HCO<sup>+</sup>. Is it caused by multiple outflows with different ages, or just single outflow changes its direction in large area? Deeper observations should be carried out to answer this question.

Assuming that HCO<sup>+</sup> (1-0) emission in the line wings to be optically thin and Local Thermodynamic Equilibrium (LTE),  $X(\text{HCO}) = [\text{HCO}]/[\text{H}_2] = 10^{-8}$  (Turner et al. 1997) and  $T_{ex} = 15$  K, we derive the column density from:

$$N(\text{HCO}) = Q(T_{ex}) \frac{8\pi\nu_0^3}{c^3} \frac{g_l}{g_u} \frac{1}{A_{ul}} [1 - e^{-h\nu_0/kT_{ex}}]^{-1} \int \tau dv (1)$$

where  $\nu_0$ ,  $g_u$ ,  $g_l$  and  $A_{ul}$  are the rest frequency, the upper

and lower level degeneracies and the Einstein's coefficient of HCO,  $Q(T_{ex})$  is the partition function, and  $c$  is the speed of light. On the other hand, by assuming HCO emission is optically thin in the line wings, we use the approximation:

$$\int \tau dv = \frac{1}{J(T_{ex}) - J(T_{bg})} \int T_{mb} dv \quad (2)$$

The derived parameters are shown in table 2.

### 3.2 Infall signatures detected by HCO<sup>+</sup> (1-0) and H<sup>13</sup>CO<sup>+</sup> (1-0)

The HCO<sup>+</sup> (1-0) spectra of four sources (figure 8) do not have a simple Gaussian shape, presenting spectral wings and absorption dips where is the emission peak of H<sup>13</sup>CO<sup>+</sup> (1-0), which suggest that the molecular gas are affected by the dynamics of these star-forming regions. Mapping observations could help us to distinguish whether this was caused by inward motions or other dynamics such as outflow, rotation and expansions of HII regions. Figure 8 (the left panels) show the mapping observations towards our four sources with double peaked HCO<sup>+</sup> (1-0) emissions. Three sources except G340.248-00.376 show consistent blue profile, indicating infall motions. Outflow activities are also detected in these regions (see section 3.1). Like low star formation mechanical, massive stars in these regions are also forming through accretion-outflow process. For G345.0034-00.2240, the detection of recent outflow activity traced by SiO and the appearance to be undergoing infall in this region suggest ongoing accretion beyond the onset of the HII region. The outward radiation and thermal pressure from the central massive star(s) do not seem to strong enough to halt accretion. Like G10.6-0.4 (Keto & Wood 2006), accretion flow in this region may be ionized.

Klaassen et al. (2007,2012) obtained JCMT observations of HCO<sup>+</sup>/H<sup>13</sup>CO<sup>+</sup> (4-3) to trace large scale inward motions in a sample of massive star-forming regions (mainly MYSOs, HCHII and UCHII regions) The infall rate in our sample is relatively low compared their work. This may be partly due to their higher resolution (15'' vs. 38''). Besides, the higher J = 4-3 transition does not self absorb as readily as J = 1-0, making it a better asymmetry tracer. Only one source in our MYSO candidates show infall signature. This is because the infall area with MYSO is relatively smaller than that in UCHII regions, and then more likely to be beam diluted.

### 3.3 A simple model of G318.9480-00.1969

G318.9480-00.1969 is the only MYSO candidate detected in-fall signatures. In this section, we try to constrain the spatial and dynamic structure of G318.9480-00.1969, using a radiative-transfer model that reproduce  $\text{HCO}^+$  (1-0) line. We employed the three dimensional radiative-transfer code RADMC-3D (developed by C.Dullemond) to compute the dust temperature heated by a central stellar and line emission of an infall model. The dust opacity is from Ossenkopf & Henning (1994) without grain mantles or coagulation. The molecular data of  $\text{HCO}^+$  comes from the Leiden LAMDA database<sup>2</sup>. The line transfer assumes the gas temperature to be equal to the dust temperature and LTE (full non-LTE radiation transfer is also planned for RADMC-3D).

In our model, the volume density follows a radial power law,  $n \propto r^{-1.5}$ , with a total mass of  $31 M_{\odot}$  (estimated from our observations) within a box of  $(4000 \text{ AU})^3$ . At the center lies a star of  $10 M_{\odot}$  (see section 3.4). The gas has a turbulence velocity of  $0.5 \text{ km s}^{-1}$  and is radially infalling with  $1.8 \text{ km s}^{-1}$  to the central star. A comparison of the observed and model spectra is shown in figure 9. At the center spectra our model matches well this the observation. However, the observed line seems to have line wing emissions, probably caused by outflow activities. The detected SiO spectra indeed imply beam diluted outflow(s) in this region. Even though our model is consistent with the data, we should realize it does not provide errors of the parameters, and different models may also fit as well.

### 3.4 Spectral energy distribution

In this section, we try to fit the spectral energy distribution (SED) of our sources using the tool developed by Robitaille et al. (2007). Briefly, the SED-fitting tool works as a regression method to find the SEDs within a specified  $\chi^2$  from a large grid of models after fitting the input data points. The grid of models contains stellar masses, disk masses, mass accretion rates, and line-of-sight (LOS) inclinations. The grid of YSO models was computed by Robitaille et al. (2006) using the 20,000 two-dimensional radiation transfer models from Whitney et al. (2003a, 2003b, 2004). Each YSO model has SEDs for 10 viewing angles (inclinations), so the total YSO grid consists of 200,000 SEDs. We use the archival data from 2MASS, IRAC of Spitzer, MSX to fits the SED of our sources.

## ACKNOWLEDGMENTS

## REFERENCES

- Bonnell, I.A. et al 1998, MNRAS, 298, 93  
 Bonnell, I.A. et al. 2004, MNRAS, 349, 735  
 Elmegreen, B. G., Lada C.J., 1977, ApJ, 214, 725  
 Foster J.B., et al. 2011, ApJS, 197, 25  
 Keto, E. 2002, ApJ, 580, 980  
 Keto, E., Wood, K. 2006, ApJ, 637, 850  
 Klaassen P.D., Wilson C.D., 2007, ApJ, 663, 1092  
 Klaassen P.D., Testi, L., Beuther, H., 2012, A&A, 538, 140

- Ladd N., Purcell, C., Wong, T., & Robertson, S. 2005, PASA, 22, 62  
 Lefloch, B., Lazareff, B., 1994, A&A, 289, 559  
 Lumsden, S. L., Hoare, M. G., Oudmaijer, R. D., Richards, D. 2002, MNRAS, 336, 621  
 Mardones, D., Myers, P. C., Tafalla, M. et al. 1997, ApJ, 489, 719  
 Molinari, S., Brand, J., Cesaroni, R., Palla, F. 1996, A&A, 308, 573  
 Ossenkopf, V., & Henning, T. 1994, A&A, 291, 943  
 Robitaille, T. P., Whitney, B. A., Indebetouw, R., Wood, K., Denzmore, P., 2006, ApJS, 167, 256  
 Robitaille, T. P., Whitney, B. A., Indebetouw, R., Wood, K., 2007, ApJS, 169, 328  
 Schilke, P., Pineau des Forêts, G., Walmsley, C.M., et al., 2001, A&A, 372, 291  
 Shepherd, D.S., Kurtz, S.E., Testi, L. 2004, ApJ, 601, 952  
 Sridharan, T. K., Schilke, P., Menten, K. M., Wyrowski, F. 2002, ApJ, 566, 931  
 Sun Yan, Gao Yu, 2009, MNRAS, 392, 170  
 Urquhart, J. S., Busfield, A. L., Hoare, M. G., et al. 2007a, A&A, 461, 11  
 Urquhart, J. S., et al. 2007b, A&A, 474, 891  
 Urquhart, J. S., et al. 2008, A&A, 487, 253  
 Whitney, B. A., Indebetouw, R., Bjorkman, J.E., Wood, K., 2004, ApJ, 617, 1177  
 Whitney, B. A., Wood, K., Bjorkman, J. E., Cohen, M., 2003a, ApJ, 598, 1079  
 Whitney, B. A., Wood, K., Bjorkman, J. E., Wolff, M. J., 2003b, ApJ, 591, 1049

This paper has been typeset from a  $\text{T}_{\text{E}}\text{X}/\text{L}^{\text{A}}\text{T}_{\text{E}}\text{X}$  file prepared by the author.

<sup>2</sup> <http://www.strw.leidenuniv.nl/~moldata>